

## RESEARCH ARTICLE

# Autonomous Energy Controller and Econometric Analysis of an Energy Reserve Generating Network

OLUWASEUN OLANREWAJU AKINTE<sup>1</sup> AND BOONYANG PLANGKLANG<sup>2</sup>

Department of Electrical Engineering, Rajamangala University of Technology Thanyaburi, Khlong Hok, Pathum Thani 12110, Thailand

Corresponding author: Boonyang Plangklang (boonyang.p@en.rmutt.ac.th)

This work was supported by NSRF under the Management Unit of Human Resources and Institutional Development Research and Innovation program under Grant BIBF660068.

**ABSTRACT** Alternative power generators form the basis for reliability, affordability, and sustainability in accessing rural and urban communities from developing or developed countries (with minimized emission of gases) in connection and isolation from the utility grid system have obviously illustrated important roles in power system. Econometrics and energy assessment of a hybrid renewable energy-power reserve network were analyzed with grid connection in Ko-Kut Island (Thailand) from this paper. Hybrid sources (solar photovoltaic energy, utility grid, biomass resources fueling biogas energy system, wind energy turbine and high energy flywheel) and a unified power reserve unit (vanadium redox flow: VRXFB, sodium sulphur: NaS, Li+: lithium-ion, ZnBr: zinc bromide flow batteries) were designed to effectively manage the energy flow linking the unified generators and the needed energy from the island. A combined dispatch energy controller was used as an interactive controller system across the generators, batteries, and load to enhance the unified energy system's flexible operation into four different configurations in order to investigate their energy cost, net present service cost, energy sales/energy purchases from the utility grid, and estimated operational cost performances, respectively. In addition, an optimized power management control algorithm was designed with microgrid power analysis software (HOMER) to determine the most economic and efficient generating system architecture. It was observed from the optimization result that the architecture of VRXFB energy system had the least energy tariff (\$ 0.1013/kWh), net current (\$2,502,038) and operational (\$58,830.93) service costs with the highest renewable energy fractional contribution of 75.0 % to the grid network, technically.

**INDEX TERMS** Control systems, econometric analysis, hybrid energy technology assessment, grid network, integrated hybrid energy network.

## NOMENCLATURE

### ACRONYM(S)

AC	Alternating Current.	HOMER	Hybrid optimization of multiple energy resources.
CO	Carbon (I) oxide.	LABVIEW	Laboratory virtual instrument engineering workbench.
CO <sub>2</sub>	Carbon (IV) oxide.	Li <sup>+</sup>	Lithium-ion battery.
Coe	Cost of energy.	LsPSPp	Loss in power supply probability.
C <sub>x</sub> H <sub>y</sub>	Hydrocarbon gas emission.	MATLAB	Matrix laboratory.
DC	Direct current.	NASA	National aeronautics and space administration.
		Na-S	Sodium Sulphur battery.
		NO <sub>x</sub>	Nitrogen oxide.
		NREL	National renewable energy laboratory.

The associate editor coordinating the review of this manuscript and approving it for publication was Alexander Micallef<sup>3</sup>.

Pb <sup>2+</sup>	Lead (II) ion battery.
PVsc	Photovoltaic system.
SO <sub>2</sub>	Sulphur (IV) oxide.
STC	Standard test condition.
VRXFB	Vanadium redox flow battery.
Zn-Br	Zinc bromide flow battery.

**SYMBOL (S)**

A <sub>cc</sub>	Annuity (\$).
A <sub>FF</sub>	Annuity factor.
A <sub>nt</sub>	Overall annuity (\$).
C <sub>gr</sub>	Utility grid tariff (\$).
C <sub>inc</sub>	Investment cost (\$).
E <sub>BGP</sub> (t)	Output energy of biogas generator (kWh).
EN <sub>bttts</sub> (t <sub>s</sub> )	Batteries present energy level (kWh).
EN <sub>bttts</sub> (t <sub>s</sub> -1)	Batteries previous energy level (kWh).
E <sub>nerdem</sub>	Energy demand (kWh).
E <sub>nerg-Fess</sub>	Energy stored by flywheel system (kJ).
I <sub>FC</sub>	Fictitious interest (%).
K	Period of planning (years).
L.C.O.E <sub>s</sub>	Levelized cost of energy (\$/kWh).
N.C.F <sub>ti</sub>	Periodic net cash flow (\$).
N <sub>gr</sub>	Grid emission forecast price (\$).
N.P.V <sub>cc</sub>	Net present value (\$).
P <sub>bat</sub>	Power capacity of batteries (kW).
P <sub>biog</sub>	Power capacity of biogas generator (kW).
P <sub>conv</sub>	Power capacity of converter (kW).
P <sub>fly</sub>	Power capacity of flywheel system (kW).
P <sub>gen</sub>	Total capacity of hybrid power sources (kW).
P <sub>grid</sub>	Grid capacity (MW).
P <sub>gridsales</sub>	Power capacity sold to the grid (kW).
P <sub>Load</sub>	Energy demand or load capacity (kW).
P <sub>Losses</sub>	Total power loss (kW).
P <sub>opp</sub>	Output power of wind turbine (kW).
P <sub>rxa</sub> (t)	Power capacity of strings of solar PV panel (kW).
P <sub>solar</sub>	Power capacity of solar PV array (kW).
P <sub>wind</sub>	Power capacity of wind turbine (kW).
R <sub>Fr</sub>	Renewable fraction (%).
SEP <sub>rxa</sub> (t)	Output Power of solar PV module (kW).
SOC <sub>bat</sub>	State of charge of batteries (%).
SOC <sub>fly</sub>	State of charge of flywheel system (%).
V <sub>ctt-in</sub> (t <sub>s</sub> )	Cut in speed of wind turbine (m.s <sup>-1</sup> ).
V <sub>ctto</sub> (t <sub>s</sub> )	Cut out speed of wind turbine (m.s <sup>-1</sup> ).
V <sub>ws</sub> (t <sub>s</sub> )	Wind energy turbine speed (m.s <sup>-1</sup> ).
NPV <sub>cc</sub>	Net Present value (\$).
η <sup>-Power-bdconv</sup>	Efficiency of converter (%).
∑ P <sub>gen</sub>	Total power generated from hybrid network (kW).
∑ P <sub>NRS</sub>	Total power generated from fossil generators (kW).

**I. INTRODUCTION**

Increasing environmental issues and fossil fuel shortage have led to boosting alternative energy supply development [1]. Solar (photovoltaic: PVsc) panel and wind plants have a wide application on the global environment [2], [3]. Energy users focus on cost minimization, profit maximization, and efficient maximization of alternative energy generators. The technological and economic estimation of energy systems in terms of their performance is a great challenge; hence, the need for a quantitative mathematical method is essential to configure the components for optimization. Presently, the evaluation of technology and economics of renewable energy systems' application is receiving much concern [4], [5]. The economics-cost benefit of solar-photovoltaic and wind plant turbines vary in their conditional resources, policies relating to local subsidies, and system components [6]. The resourceful, environmental, and econometric aspects have been quantified comprehensively under few studies, thereby hindering renewable energy systems usage due to research limitations. In terms of demand, emission, and safety, pressure from the environment is responsible for continuous renewable energy concern, which has led to numerous operations on energy systems for practical use. Energy management, stability control, and uninterrupted power flow are highly essential for an efficient power system network to operate successfully in the world [7]. The need for energy assessment will focus on the rate of energy consumption and losses in a hybrid power network when energizing electrical devices like lighting systems, electromagnetic equipment, industrial appliances, heating systems, commercial appliances, etc. Security in energy supply can be improved through storage systems and the distribution of various power generation sources which can reduce impacts on the environment [8]. Hybrid power generation sources including solar PVsc, wind power turbines, downdraft biomass gasifier-biogas generators, and hydropower turbines have improved the health of the environment in relation to emission reduction, distribution of electric power systems, and clean energy production [9].

The present and previous research studies seek the maximization of economic benefits of sustainable resources [10], [11], it also investigates feasible analysis by assessing remote and urban electricity sectors across the world with disconnected grid and grid-connected hybrid alternative power system application. Razmjoo et al. [12] researched on some significant indicators impacting renewable energy and the environment by reducing CO<sub>2</sub> emissions and providing investment as a guide to energy system achievement with optimization through case analysis of renewable energy systems [13]. Cuesta et al. [14] conducted a study on job creation as a social parametric framework tool to optimize the hybridized renewable generating source as a wider aspect of the environment or society. Fodhil et al. [15] gave a report on the particle swarm optimization slight delivery of lower energy cost (coe valuation of \$0.38/kWh) in comparison to HOMER coe valuation of \$0.40/kWh during the

simulation analysis of the hybridized generators' network. The hybridized solar PVsc plant, wind power turbine, and batteries configuration provided an analogous coe valuation of \$0.508/kWh when optimized with genetic-particle swarm optimization algorithms and provided a coe valuation of \$0.51/kWh when optimized with HOMER as an observation from Ghorbani et al. [16]. Eltamaly et al. [17] compared the cost of energy result obtained from hybrid architecture of solar PVsc plant, wind power generator, conventional generator, fuel cell generator, and batteries energy system through the application of particle swarm optimization algorithm with a coe valuation of \$0.2805/kWh and HOMER with a coe valuation of \$0.2774/kWh. A technological-economic report assessment from the hybrid configuration of solar PVsc, wind power turbine, and batteries based energy system from a remote island was conducted by Javed et al. [18] through the use of genetic algorithm optimizer technique from the toolbox of MATLAB optimizer and the result was compared with HOMER energy grid software to reduce or minimize the cost of electricity within a reliable index certainty and a comparable result between the genetic algorithm and hybridized optimization analysis of modelled multi-energy resources (each having different sizing alternatives) was obtained. Jamshidi and Askarzaden [19] configured and sized a hybrid solar photo voltaic generator, fuel cell, and diesel plant energy system by using a crow multiplex-objective search algorithm to consider its supply from a power loss probability and net present cost's value. Ramli et al. [20] sized and optimized a hybrid configuration of a solar PVsc, wind generator, diesel generator, and batteries energy system by minimizing its energy valuation and increasing its reliability through the adoption of a multiple-objective-auto-adaptive differential evolutionary algorithm. A major concern to the rural community is reliability in electric power supply towards it (rural community) due to unlikely connection from the utility grid network because of constraints in technological facilities within the rural area. Hence, selecting a suitable index on reliability is essential for sizing components accurately on energy system.

Li et al. [21] configured a hybridized solar plant energy, wind power turbine, and biogas energy generating system for a load demand within a community and discovered the hybridized system can produce electric power for the consumers at a valuation of \$0.201/kWh (electricity cost). Several energy resources are embodied by the hybrid generators network which enhanced the generating systems reliability in comparison with a single energy source in terms of power delivery and supply in energy system distribution. The engrossed effort towards advancing hybrid energy system and energy storage technologies for cost-effectiveness and efficient transfer of electric energy supply to remote and isolated areas is still in progress. Many feasibility studies on hybrid energy systems with their sizing analysis for electric power supply to remote areas (off-grid) have been carried out. Arévalo et al. [22] analyzed vanadium flow

battery (redox VRXFB) without considering its life cycle emission. Concluding that the redox flow VRXFB has a lower energy cost and higher life cycle than the lead ( $Pb^{2+}$ )-acid and lithium ( $Li^+$ )-ion batteries. Argyrou et al. [23] stated the challenges behind the continuous replacement of lead acid ( $Pb^{2+}$ ) batteries in remote areas due to limitations in their lifetime with current research. Lithium ( $Li^+$ )-ion batteries possess 500-2000 W/kg power densities, higher efficiencies range (90.0-97.0 %) with a fast time response (lesser than  $5 \times 10^{-3}$ s). Relating capital investment and lifetime between lithium ( $Li^+$ )-ion and vanadium flow batteries, Arévalo et al. [22] discovered that more capital investment is required on the  $Li^+$ -ion (lithium) than the VRXFB battery. While VRXFB has higher lifespan than the lithium ( $Li^+$ )-ion battery. For standalone usage with respect to higher lifetime, VRXFB technology is an adequate contender. The fast time response of VRXFB is rapid when related to loading variation and has undergone wide development in renewable energy systems' applications. Aneke and Wang [24] illustrated high tolerance of batteries during their overcharging operation which requires low cost of maintenance, low operational cost, and full discharge to 100 % (depth) with no negative effect on the batteries' life cycle. Nguyen and Savinell [25] stated the required facilities needed for a VRXFB storage system which are controlled instrument, power flow management, and pumping configuration, respectively. Making it bit challenging for the requirement of operating low energy storage systems. The hybridized energy configuration of solar plant, wind power turbine, and batteries possesses life cycle emissions without operational emission due to energy production, energy transportation, and operational cradle component of the energy system. Most research did not give the life span (cycle) emission of the alternative energy systems' component during sizing of the hybrid power network configuration, rather their investigation was carried out by applying a metaheuristic approach (non-dominating sorted genetic algorithm II) from Huang et al. [26], adapting referenced point base multi-objective evolutionary algorithm from Liu et al. [27] and scenario-dominating base algorithm from Wang et al. [28]. Few reports from researchers on life cycle emission during the system component design as an objective function was done.

Brka et al. [29] presented a sizing configuration report of a solar plant, wind power turbine, fuel cell, and batteries hybrid energy network through the incorporation of a multiple-objective genetical-algorithm optimizer which considers the objective functions of net present costs, life cycles' emission, and excess energies. Mayer et al. [30] researched on a single, multiple, objective genetic algorithm optimizers of a hybrid configuration of solar PVcs energy, wind power generator, and batteries alongside a household solar collector producing electricity and demand for hot water through minimization of net present cost and life cycle emission's value. Also, Barakat et al. [31] optimized a unified configuration of solar PVcs energy, wind power generator, and batteries connected

to a grid network by using a multiple-objective particle swarm optimization algorithm. The energy cost, power loss supply probability, and fraction from renewable energy systems were considered objective functions while life cycle emission was evaluated as a parameter of consequence. Current researchers minimized the life cycle emission and cost of electric energy for a sized optimal hybrid configuration of solar energy PVsc plant, wind power turbine, biogas plant, and vanadium (redox flow) battery network with a reliable index of power loss supply probability ( $L_sPSPp = 1.00 \pm 0.005$ ) through the application of single, multi-objective genetic algorithm optimizer technique whose result was compared with output result of HOMER power tool. The preceding literature review indicated the configuration of solar energy PVsc plant, wind power turbine, and biogas energy system rarely use VRXFB or was not studied appropriately. Sarkar et al. [32] hybridized a configured solar energy PVsc, wind power turbine, biogas generator, and VRXFB energy system using HOMER power software to consider the functional reliability and analyze its cost only. The previous research applied the single and multiple objective genetic algorithm to determine the energy cost and life cycle emission and both results were compared with the HOMER power tool. The present researchers applied a multiple-objective genetic algorithm optimization to investigate the hybridized configuration of solar energy PVsc, wind power generator plant, biogas energy generator, and VRXFB energy system with an applied life cycle emission for the components of hardware in consideration of the hybrid configuration as an objective function from Das et al. [33]. Furthermore, Das et al. [33] experimented on a hybridized solar energy PVsc, biogas, and batteries energy system for a load demand in Bangladesh within a remote Island of Saint Martin. Kumar et al. [34] analyzed the hybrid configuration of solar plant, diesel generator, and batteries energy network from a technological economic value and environmental feasibility' report view to have produced the most optimized solution result when compared to the configuration of solar plant, diesel generator, wind power turbine, and batteries energy network from the southern part of India.

Sifakis et al. [35] studied different dispatch strategies with their effective performance on seaport which was connected to the grid hybrid energy network with their storage categories. Wang et al. [36] performed an experiment on hybridized configuration of solar energy PVsc, wind power turbine, and batteries that was connected to the grid to energize a plant for water treatment through the application of LINGO software tool. Samy et al. [37] obtained the architectural optimization of hybrid fuel cell energy and biogas energy network in which the primary source of energy generation was biogas, and the backup energy supply was a fuel cell. Eisapour et al. [38] experimented on a hybrid-smart energy network at Shiraz University (Eram campus) using the HOMER power tool to attain heat and energy demand. Kaur et al. [39] optimized two different configurations of mini-grid systems and concluded that the hybrid solar plant

and biogas microgrid energy system performed a better optimization result for Punjab rural areas with a low energy valuation of \$0.0735/kWh. Gebrehiwot et al. [40] discovered that the hybrid solar plant, wind power turbine, and diesel plant energy system was more reliable and efficient to electrify Ethiopia's remote areas. Malik et al. [41] discovered that introducing a biomass gasifier system to a hybrid solar plant and wind power plant energy network will satisfy the load demand of a building. Tariq [42] compared two different hybrid configurations and discovered that the hybrid renewable energy referenced system with renewable resources can reduce diesel consumption from 65.78 to 0.53 % of its valuation share. Nazir [43] proposed a hybrid solar plant, grid, and battery system to supply electric current to railway track systems moving at a high speed. Parihar et al. [44] studied a hybrid alternative energy-biomass-based system and discovered that the biogas and battery configuration was economically preferable when compared to a standalone energy system. Aziz et al. [45] investigated the viable analysis of a distinctive hybrid renewable system and concluded that the hybrid solar plant, hydropower plant, diesel generator, and batteries are the best alternative in terms of catering for load demand from the rural village of Iraq. Baruah et al. [46] performed experiment on the analysis of a hybridized renewable energy network to electrify an institution town in India (east district of Sikkim). They discovered that the hybrid solar plant, biomass generator, micro hydropower, and batteries energy system produced \$0.095/kWh (low energy valuation) electric cost as the most economical energy system. Sinha and Chandel [47] Sinha and Chandel [48] proposed an integrated energy resources system for sites with low wind pressure in India (Himalayan area). Malik et al. [49] reviewed extensively a biomass-based hybrid energy system capable of environmental sustainability and cost-effectiveness in rural areas as an option. The global application of a well-developed power tool software for optimizing and sizing integrated hybrid energy system networks are HOMER PRO, LABVIEW, MATLAB SIMSCAPE and SIMULINK, NREL, HYBRID 2, etc. In which HOMER power grid analysis software provided the most efficient simulation result for the grid dependent and independent (off-grid) connections of the hybrid generators' configuration in terms of low electricity cost, net current cost value, project feasibility and future outcome [50], [51], respectively. Tsai et al. [52] investigated a feasible technical-econometric analysis of 3 different energy systems' configuration (diesel plant-solar PVsc, Li-ion battery, diesel plant/solar PVsc, independent solar PVsc/Li-ion battery plant, and independent diesel plant for an island in Pratas located in Taiwan. They discovered the configuration of diesel plant and solar PVsc system had the lowest energy valuation of \$0.357/kWh with an overall peak solar PVsc potential of 200 kW, excess energy of 2.6 % and 15.3 % of energy contribution from the solar PVsc. Ayan and Turkay [53] evaluated the environmental, econometric and technical operation of diesel plant/solar

PVsc/Li-ion/wind and wind/solar PVsc/grid hybrid energy systems for 7 different regions within the 21 states of Turkey by adopting HOMER energy grid to analyze the energy cost, emissions from greenhouse gases, optimal energy system architecture, net current cost and energy fraction from alternative energy system. The net current cost varied in boundary (\$23,372-\$40,858) for the diesel plant/solar PVsc/Li-ion/wind system and varied in boundary (\$2,540-\$8,951) for the wind/solar PVsc/grid system. As the capital cost of wind generator and panels of the solar PVsc varies, their net current cost changed in boundaries (\$21,402.30-\$29,978.9) for diesel plant/solar PVsc/Li-ion/wind system and varies from \$37,518.1-\$51,939.0 for the wind/solar PVsc/grid system at Canakkale and Artvin states, respectively. Güven et al. [54] implemented a solar PVsc/diesel plant/wind/Li-ion hybrid power system by adopting a unified metaheuristic method (hybrid firefly novelty, genetic, particle swarm optimizer, and firefly algorithms) with the energy system design in Turkey for a university campus to optimize the unified energy system's sizing. Shafiullah et al. [55] performed a technical and econometric analysis of a unified solar PVsc/diesel plant/hydropower/lead acid system in Zimbabwe (rural Chipendeke community) by adopting HOMER energy analysis and considering operation for 6 varieties of the unified energy system's configuration (solar PVsc/lead/hydropower system, hydropower system, solar PVsc/lead/diesel/hydropower system, lead/diesel/hydropower system, diesel/hydropower/lead system and diesel/hydropower system). The solar PVsc/diesel/hydropower/lead system produced the most feasible econometric values of energy cost: \$0.165/kWh and net current cost: \$307,657. Iqbal et al. [56] developed a solar PVsc/utility grid/Li-ion batteries system for 3 universities in Pakistan (Muzaffaraband university, campus of king Abdullah and Kashmir/Azad Jammu University) by using HOMER energy simulation and comparing their energy cost from the grid connected source in existence when generating equal power flow towards the consumer. The grid connectivity system's energy cost was \$0.33/kWh which was minimized to \$0.0030/kWh by the solar PVsc plant by concluding that the grid/solar PVsc/Li-ion batteries system was the most efficient energy system in comparison with other energy system's architectural design (grid/solar PVsc/diesel plant/batteries and diesel plant/grid systems). Habib et al. [57] focused on utilizing the optimization of two hybrid energy system configurations (solar PVsc/biogas plant/wind/batteries and solar PVsc/biogas/super conduction magnetic storage systems) as an independent microgrid network system operating in a rural area to reduce the overall net current cost, energy cost and toxic emissions by adopting a hybrid integer linear programmer and MATLAB software (Simulink).

This paper addresses an interfacing unified dispatch strategy (combined dispatch, cycle charging, load monitoring) with a multi-flexible capacity operation over the modelled hybrid generators (biogas/solar/grid/wind/flywheel), hybrid batteries (Zn-Br/Na-S/Li-ion/VRXFB) and load to

verify the best feasible econometric and technically efficient network provider from four different architectural energy systems (solar/wind/biomass-gasifier/VRXFB/flywheel/grid, solar/wind/biomass-gasifier-biogas/flywheel/ZnBr/grid, solar/wind/biomass-gasifier-biogas/flywheel/NaS/grid/converter and solar/wind/biomass gasifier-biogas/flywheel/Li+/grid/converter), respectively.

The previous literature review recommended various architectures of the hybridized renewable energy system for rural and urban environments with much emphasis on solar energy PVsc, wind power plant, diesel generators, and Li-ion-lead acid batteries. The architecture of solar PVsc/wind generator/biomass gasifier generator/high frequency flywheel generators and Zn-Br/Na-S/Li-ion/VRXFB batteries (integrated storage system) is yet to be investigated and identified from the previous literature review and current research. The hybrid generating network uses a combined dispatch energy strategy (as a central control system) that can assign the appropriate strategy (either load following or cycle charging energy controller) for the network architectures to deduce the best technical, economical, and efficient energy system mode during electrification, energy conversion, energy utilization and tariff management (econometric analysis) between the utility grid and microgrid architecture. Depending on the productive capacity of the wind power, solar PVsc, and utility grid generators, the central control system can program the load (energy demand) following and cycle charging energy controllers to allow the energy sources of the network to operate simultaneously. The designed hybrid energy system will utilize the power sources and power reserve unit to operate as short and long duration services between the AC loads and grid network system, respectively. The hybridized energy system will exercise control over the electrical strain effect between the clean (renewable) sources and the utility grid network. The entire network system will prevent capacity shortage by meeting the AC load requirement and enable the power reserve unit to supply more energy than the required load demanded as a means of a reliable system network for Ko-Kut Island.

The organization of the proposed power network design for proper investigation entails the following steps: the strategic method, material application (resources), mode of operating the energy system, profile of energy demand, algorithm design, and modelling components of the power network design in Ko-Kut Island was addressed in section II. Section III described the econometric estimation in terms of net present value, average cost of energy, and annuity factor of the integrated power network operation design. Analysis of technical and econometric performance of the power network design was highlighted in section IV and the conclusion remark was finalized in section V.

## II. MATERIAL APPLICATION AND METHODOLOGY

The schematic design for the hybrid generators network with HOMER power grid application was selected to diminish the effect of electric strain from the utility grid through ancillary

supporting services from the renewable generators, enhancing multi-flexible operation of the unified network and to determine the most efficient network system from the flexible modes of the energy system architectures with reference to their grid sales/grid purchases/investment return/internal return rate/payback period for Ko—Kut island. Fig. 1 indicates the utility grid, solar PVsc plant, and wind generator as the main sources of energy while the downdraft biomass gasifier plant and electromechanical flywheel function as a support (secondary generator) to the solar PVs and wind turbine plants if the utility grid is not available and the solar-wind plants are operating below capacity in order to ensure continuity in power supply as a backup plan. The biomass gasifier generator, utility grid, wind power turbine, and solar max PVsc grid monitoring-central dedicated inverter (DC to AC conversion) supplies alternating current (AC) directly to the AC bus which conveys it to the AC load for consumption by the large commercial and utility scaled projects in Ko-Kut Island.

The batteries (VRXFB, NaS, Li-ion, ZnBr) store excess energy from either the utility grid, renewable energy plants, or the rotating mass high energy frequency flywheel (which operates as an AC generator and AC motor for energy storage and energy supply support). They (batteries) assist the hybrid energy sources in power supply when their (renewable energy sources) operating potential is below the load capacity. The storage unit (VRXFB, ZnBr, Li-ion) of the system design is suitable for medium and long-duration services while Li-ion, NaS and flywheel are also suitable for short-duration and medium duration services when the primary energy sources are below operation, thereby, making the entire energy system network more reliable with minimized losses before the main electric energy sources are restored to their normal operating potential. Fig. 2 and Fig. 3 depicts the multi-control decision-making algorithm for the hybrid generators' system management with econometric terms: internal return rate, investment return, the payback period from invested energy sources, the graphical relationship between the cumulative nominal cash flow and projected years, cost summary (net present costs, initial capital invested, operation/maintenance costs, levelized electric power cost) and power optimization result of the integrated energy network.

### A. KO-KUT ISLAND

Ko-Kut Island is at the eastern gulf of Thailand with limitations in infrastructural facilities and the main occupations/sources of income are agriculture, fishing, and tourism. Its geographical coordinates are Lat 11°39'N and Long 102°32'E respectively. Ko-Kut Island has 6 villages with a population of 3000 inhabitants, a coverage area of 162.2 km<sup>2</sup> and a terrain elevation of 59 m. The area of this Island is surrounded by 70% tropical rainforest, coconut trees, and seaside villages. Their main source of electricity is diesel power plants while the inhabitants make use of coal, kerosene, and biomass resources (wood from the forest) for heating, lighting, and

cooking. Ko-Kut area possesses a high potential for solar radiation, wind density, and biomass resources [58].

### B. LOAD PROFILE ESTIMATION: WAREHOUSE, COMMERCIAL AND DEFERRABLE LOADS

The load profile (daily, seasonal, and yearly) for the mini-industrial, commercial and deferrable load consumption within the Island territory has a daily energy consumption of 1,247.7 kWh/day as the average value, a mean power of 51.99 kW, amplitude power (peak) of 188.18 kW from the month of August and a load factor of 0.28 with a random variable noise of 31.04% on daily basis from the warehouse in Fig. 5. The commercial load from Fig. 6 consumed more energy than the industrial load with a daily energy consumption of 2426.40 kWh/day (as a mean value) and mean power value of 101.10 kW. An amplitude (peak) power value of 405.71 kW occur in the month of July with a load factor of 0.25 and a random variable noise of 10% on daily basis. An indication that more activities and energy production was involved at the commercial environment than the mini-industrial environment of Ko Kut Island.

The algorithm of the integrated energy network management system from Fig. 3 comprises of the excess power mode, power shortage mode 1, power shortage mode 2, and power shortage mode 3 operations. Under the excess power mode, the generated capacity from the power sources is more than the demand capacity. The excess power generated after fulfilling the demand capacity will be transferred to the utility grid network for sales provided the batteries and flywheel maximum energy intensities are 100 %. If the batteries and flywheel maximum energy intensities are below 100 %, the power sources will charge the storage systems (batteries and flywheel) to attain their peak energy intensities of 100 %. Under the power shortage mode 1, the power source capacity is not greater than the demand capacity, which means the power source capacity is either lesser than or equal to the demand capacity under this conditional mode. If the renewable sources (solar PVsc and wind turbine: due to their unstable resources from solar irradiation and wind speed) including the biogas generator produce the exact capacity to fulfill the demand capacity, then the generated capacity equals the demand capacity under this condition. Provided the flywheel contains no stored energy (energy level = 0) and the batteries minimum energy intensity is below 20 %. The flywheel and batteries will not be charged because the renewable generators only supplied the required energy for consumption while the utility grid is on a standby mode. The power shortage mode 2 condition state that if the renewable generation capacity is lower than the demand capacity with the batteries minimum energy intensity still below 20 % and no stored energy in the flywheel system, the utility grid will provide energy support to satisfy the demand and then proceed to store energy in the flywheel and batteries, respectively. When the renewable generation capacity is lower than the demand capacity and if the minimum energy intensity of

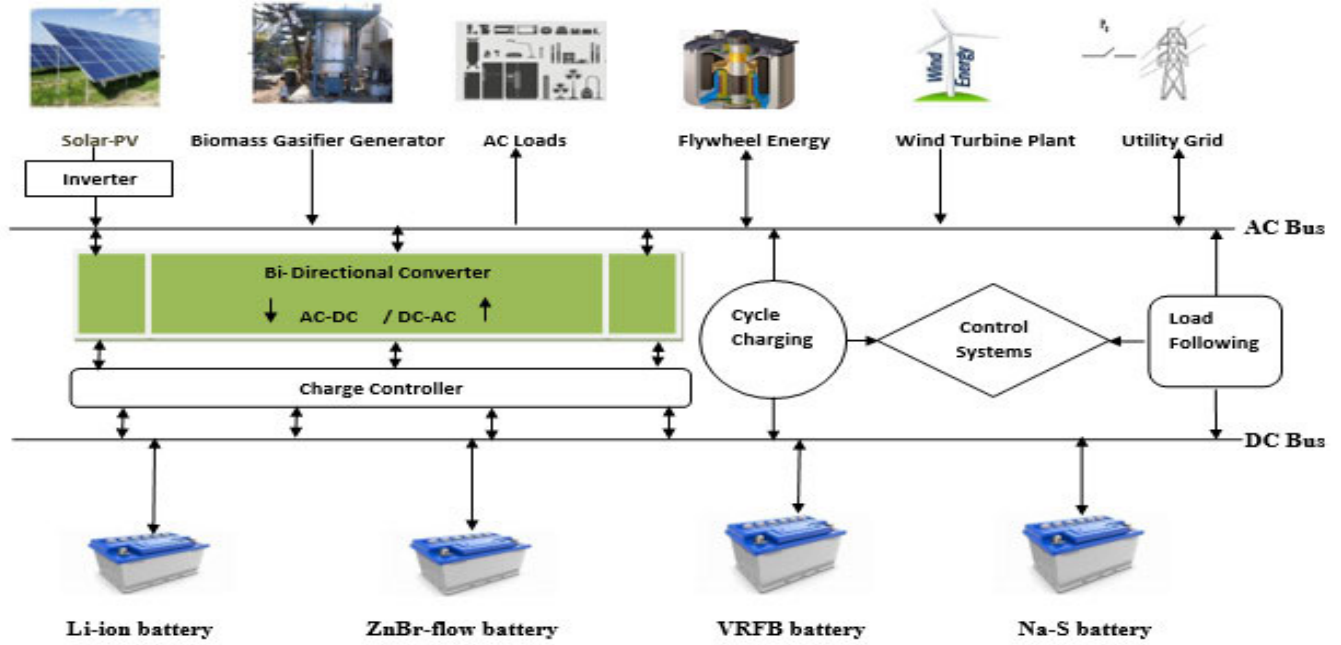


FIGURE 1. Schematic design of integrated energy-power reserve network.

the batteries dropped below 20 % and the flywheel system stores energy under the power shortage condition of mode 3, the flywheel system can discharge to support the batteries and load. However, if the batteries energy intensity is above the minimum level (> 20 %) and the flywheel energy intensity equals zero, the grid system will sell power to the microgrid network to boost power production supply for the demand and charge the storage systems (flywheel and batteries) effectively. This is how the designed network can perform flexible operation without power outage.

The mathematical expression for the load factor and average power of the mini-industrial, commercial, and deferrable loads are stated below:

$$\begin{aligned} \text{Load factor} &= \frac{\text{Average Power(kW)}}{\text{Peak Power (kW)}} \end{aligned} \tag{1}$$

$$\begin{aligned} \text{Average-Power (kW)} &= \frac{\text{Total energy consumed(kWh)}}{\text{Total period of energy consumption per day (hours)}} \end{aligned} \tag{2}$$

The potential resources (solar irradiation intensity) of Ko-Kut island is suitable enough for the feasible implementation of solar photovoltaic system to perform operation on the island. When the sun radiate light to the environment (Ko-Kut island), the radiated light experiences change in speed (refraction) and irregular (scattered) reflection as it passes through different medium of Ko-Kut atmosphere. This type of irradiation is an indirect beam of light (not directly from the sun beam) penetrating the horizontal surface of Ko-Kut island known as global horizontal irradiation of Ko-kut island with an energy density (intensity) value of 1702.7 kWh/m<sup>2</sup>. The direct sun beam from the sky penetrating the surface of Ko-Kut island (per unit area) perpendicularly without

reflection or diffraction of the sun irradiation is known as the direct normal irradiation of the island having annual energy density (intensity) of 1144.7 kWh/m<sup>2</sup>yr. The topographic view of Ko-Kut island is an important factor that accounts for the magnitude of solar irradiation intensity penetrating the surface of the island. The shadows, orientation aspect/gradient, and elevation differences are the features of the Ko-Kut island topographic view that influences the annual topographic view intensity (1406.6 kWh/m<sup>2</sup>yr) of the island, respectively. The calculation of global horizontal irradiation from the island can be estimated from the sum of the diffuse (scattered) horizontal irradiation and inclined direct normal irradiation.

Generally, the primary loads (electrical loads) are the devices that are electrified and energized by electricity. Deferrable loads (electric heater element, water pumping machine) are also electrical loads requiring some quantity of energy at a particular period. They (deferrable loads) are associated with the storage units in the schematic design of the integrated energy network when the primary energy sources have satisfied the primary load requirement and charged the batteries/flywheel into full mode. The excess electricity remaining will be consumed by the deferrable loads and the grid energy network. Figure 7 provides the average monthly consumption of the deferrable having a storage capacity of 492.75 kWh, a 30% minimum load ratio with an annual load consumption of 1.3525 kWh/day as the average value. In October, the deferrable loads had a peak load consumption value of 1.950 kWh/day as depicted from the histogram above (from Fig.7). The average power consumption of each load (industrial, commercial and deferrable) is the ratio or fraction of total energy consumed by each load (measured in kWh)

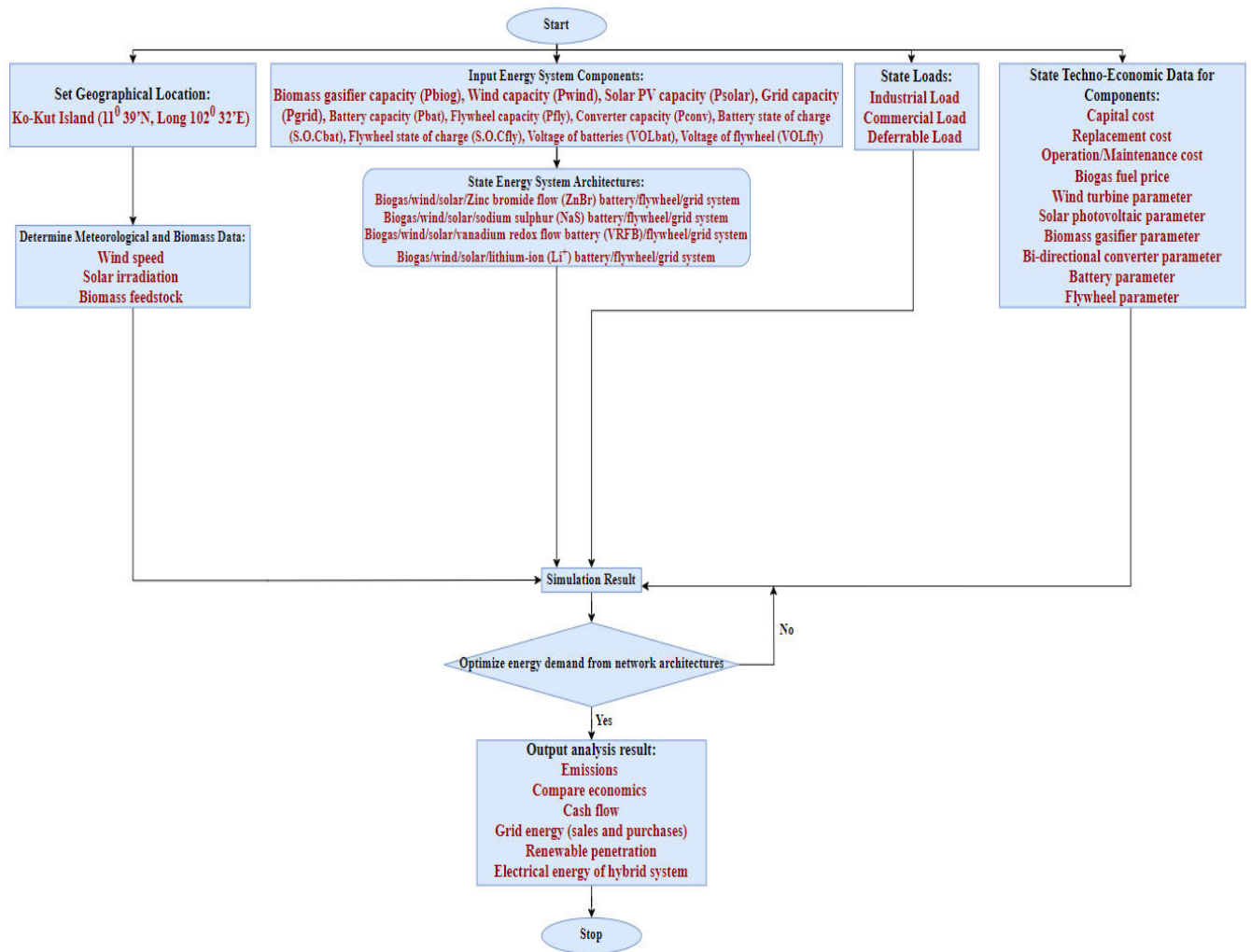


FIGURE 2. Algorithm of HOMER microgrid energy.

to the total period of energy consumed per day (measured in hours) by each load.

**C. UTILITY GRID, BIOMASS GASIFIER, WIND TURBINE, AND SOLAR RESOURCES**

The data for biomass potential resources in Ko Kut island was obtained from the datasheet base of biomass (potential) resources in Thailand (Energy Ministry: Alternative Energy Department, Efficiency and Development) while the solar energy and wind potential resources was obtained from the National Solar Radiation’s Database (NREL) and prediction estimation of NASA on global energy resources of industrial HOMER Pro analysis on microgrid power. The designed specification of the solar PVsc, biogas generator, and wind turbine was customized by the researchers according to the primary data (load requirement) source of Ko-Kut island. The specification design of the batteries and flywheel system was obtained from data sheet of the industrial HOMER PRO microgrid analysis system which is compatible with the energy demand and operate effectively with the generators capacity. The hybrid energy resources such as oil,

coal, methane gas, solar irradiation (with hydrokinetic, wind, and hydropower providing electricity through mechanical energy conversion from the turbine system) produced electric energy which was regulated, transmitted, and distributed to the consumer (energy demand) unit known as the grid energy network from Figure 1. The excess power flow cost for the national generator’s (grid) network is: \$ 0.150 per kWh while the charging cost for net excess flow from the grid network is \$ 0.050 per kWh with a yearly energy purchase from a meter reading (smart meter) of the microgrid network.

The modelled energy tariff equation from the utility grid with reference to cost signal from the utility network (grid) can be evaluated below.

$$C_{gr} = \sum_{t=1}^T [M_{grc}(t) - M_{grs}(t)] \times e_n(t) \quad (3)$$

where  
 $C_{gr}$  = Energy tariff from the utility grid (\$)   
 $M_{grc}(t)$  = Electric power bought by the microgrid system from the utility grid at a specified time (kW)



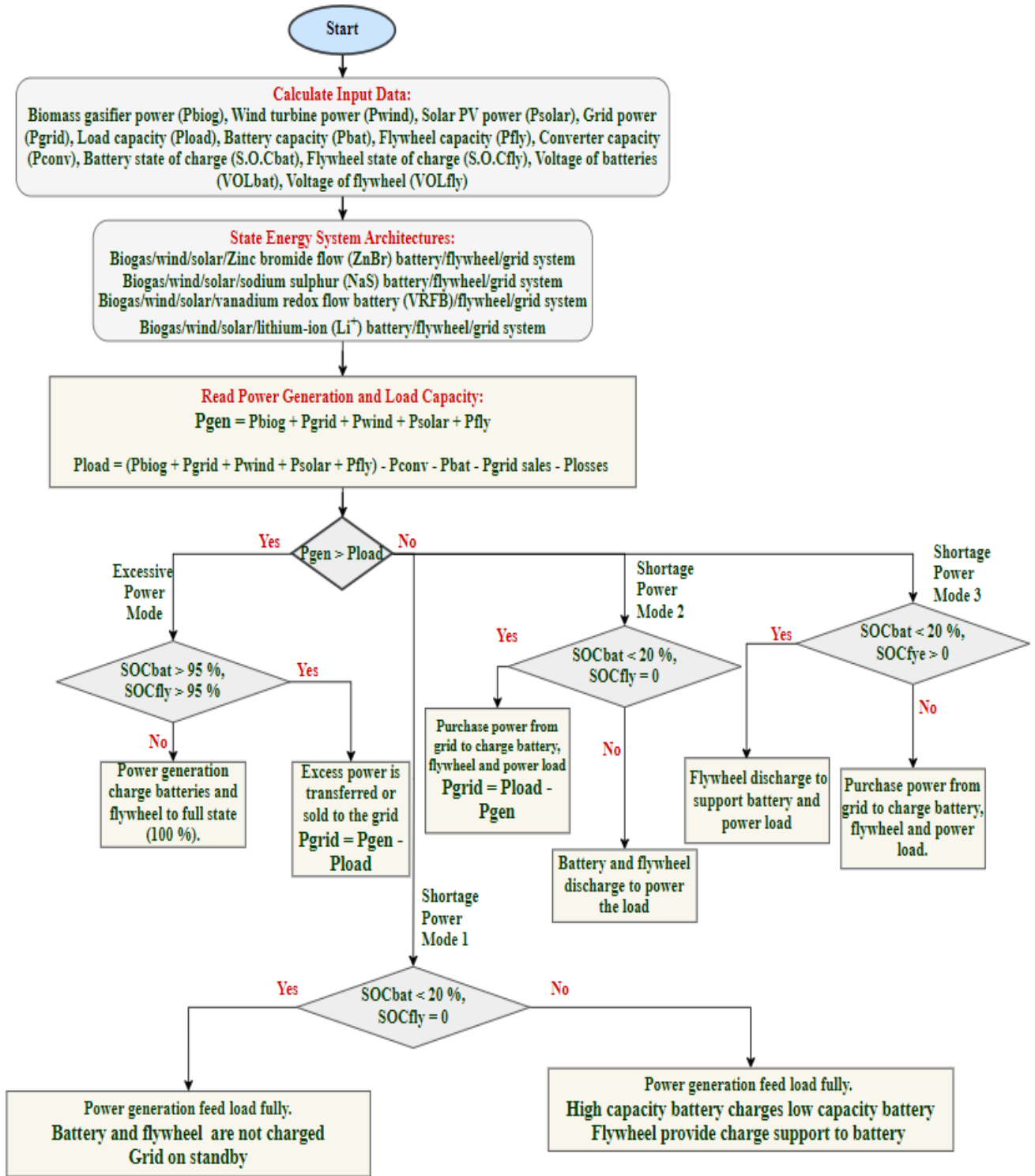


FIGURE 3. Algorithm of the integrated energy network management and emergency period.

$M_{grs}(t)$  = Excess electric power production from the microgrid system trafficked to the grid network (kW)

$e_n(t)$  = Utility grid tariff per unit (\$/kWh).

The forecast price of emission expected from the utility grid and microgrid network can be completely described by

the equation below.

$$N_{gr} = \sum_{t=1}^T [\sigma \times (M_{grc}(t))^2 + (\xi \times M_{grc}(t)) + \tau] \quad (4)$$

where

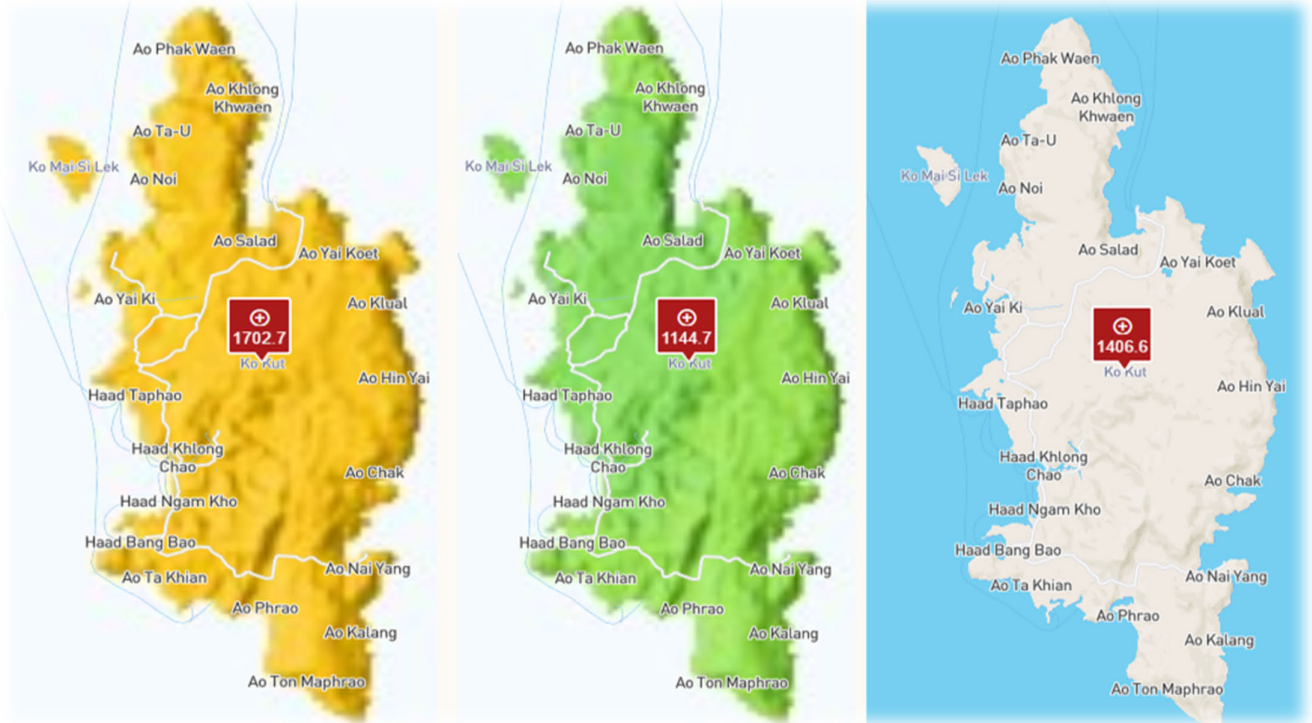


**FIGURE 4.** Global horizontal irradiation;1702.7 kWh/m<sup>2</sup>, direct normal irradiation;1144.7 kWh/m<sup>2</sup>yr, topographic view;1406.6 kWh/m<sup>2</sup>yr; solar insolation potential of Ko-Kut Island [58].

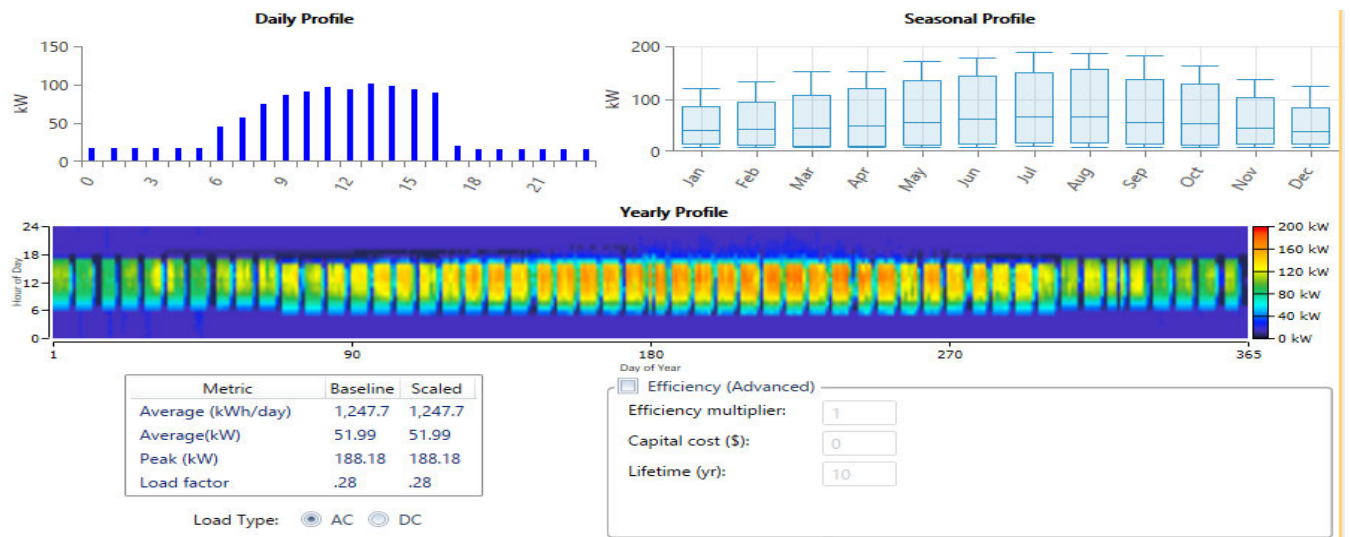


**FIGURE 5.** Warehouse load consumption.

- $\sigma$  = emission factor during grid purchase,
- $\xi$  = emission factor during grid sales
- $\tau$  = emission factor of the utility grid network [60].

The power purchase between the microgrid system (smart grid) and the utility grid provider creates a contract agreement between the two energy sources. The signal (tariff communication) from the utility grid system and the degree of energy production between the smart grid and utility grid

determines the magnitude of power purchased or sold to the grid system. When the tariff signal from the utility grid is low and energy production from the utility grid is higher than the energy production from the smart grid (microgrid) system, the grid system will be at economic merit to sell electricity to the microgrid system. If the tariff from the grid system is high and power production from the microgrid system surpasses the utility grid production, the microgrid will be at

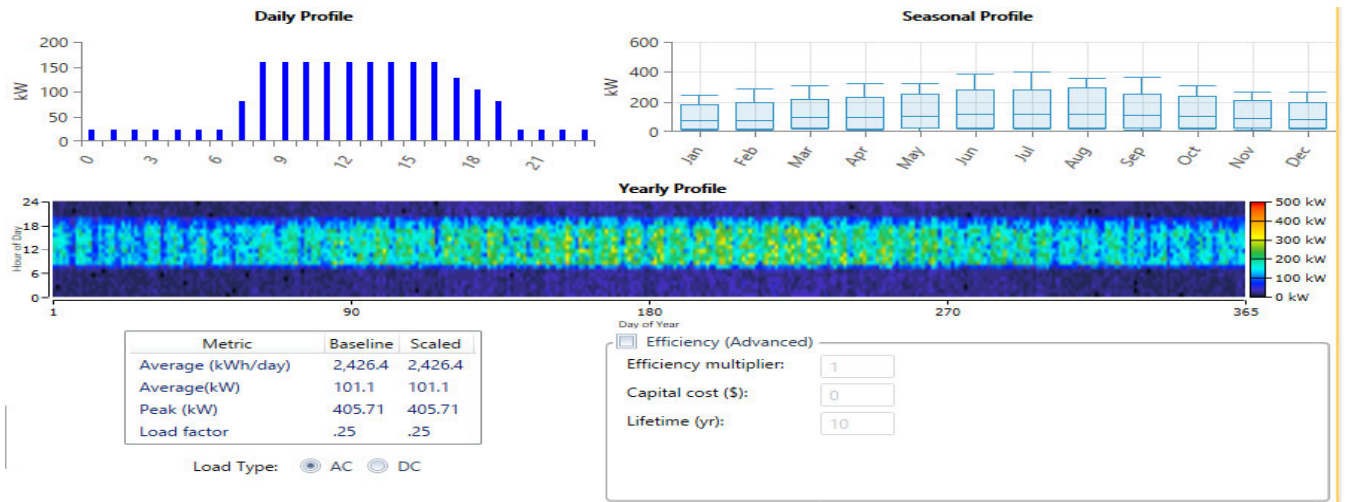


FIGURE 6. Commercial load consumption.

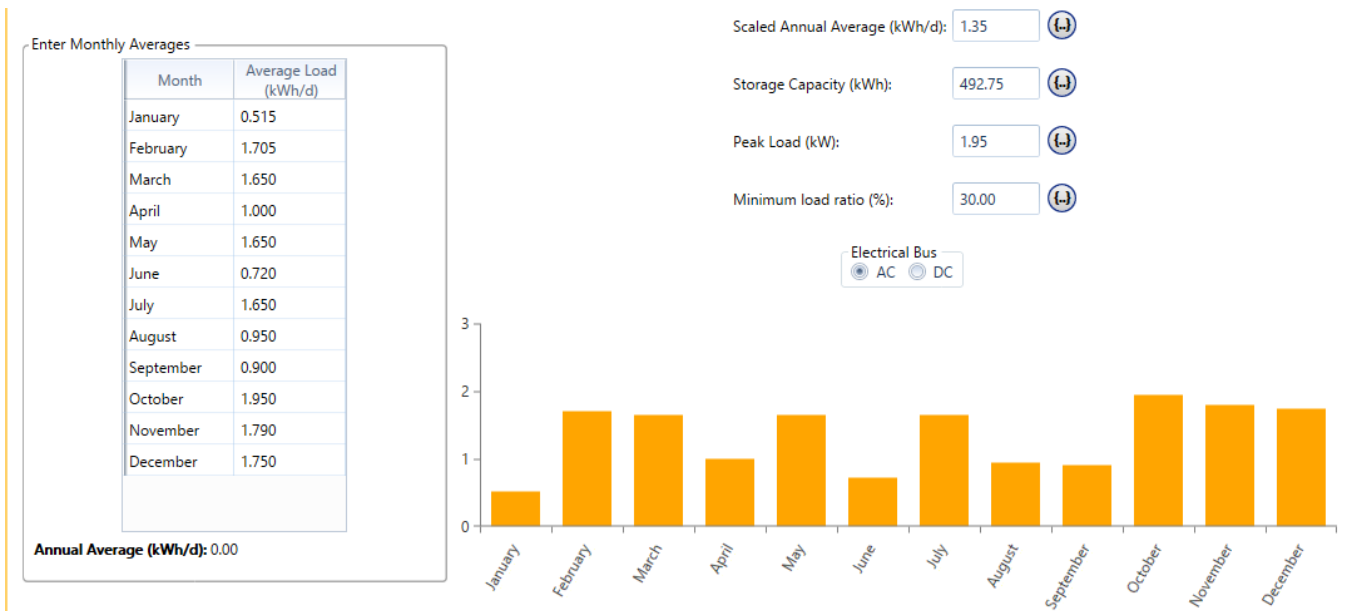


FIGURE 7. Deferrable energy.

economic merit over the utility grid system. Thereby, selling excess power to the utility grid system instead of purchasing power from the grid network. If the grid tariff is high and grid production surpasses the microgrid production, the grid still experiences economic merit over the microgrid system, thereby, selling electricity to the smart grid system at unfavorable price. In addition, the power purchased from the grid system can be stored and utilized properly when capacity shortage occurs from the generators and when energy production from the microgrid is more favorable than the grid production. During grid sales and grid purchase transaction between the utility grid and smart grid (microgrid) systems, gas emission occurs as another important factor to be considered during economic estimation between the two different

network sources known as the forecast price of emission modelled from equation 4.

1) MODELLING SOLAR PHOTO VOLTAIC GENERATION

A monocrystalline solarmax 500 RX photo voltaic 350 W module rated capacity of 500 kW with a dedicated inverter of 500 kW was used in the schematic design of the integrated hybrid energy source having a 2-axis tracking system and 20% ground reflectance. The solar max-grid following centralized inverter system will boost the power source feeding the AC bus connector, minimize losses through an inbuilt power electronic device (IGBT) of the solar PVsc-inverter system, harness current production that can be utilized from the solar irradiation. The solar PVsc-inverter

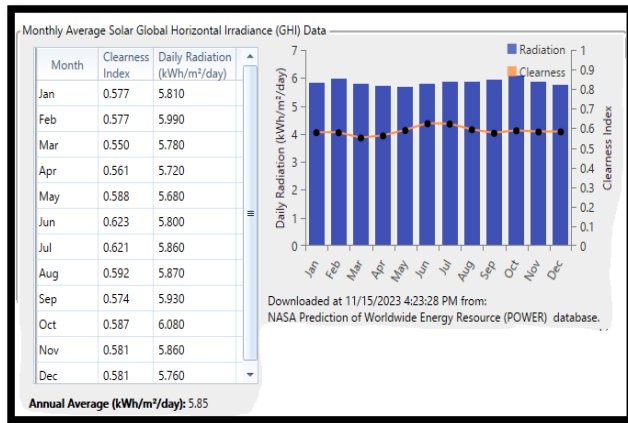


FIGURE 8. Monthly mean solar horizontal irradiation for Ko-Kut Island [61].

system will maximize the output energy production from the solar irradiation, perform effective communication with the utility grid network, monitor the output energy of the solar PVsc-inverter system and will enable fault detection that can cause damages to the solar PVsc system. The variation of incident sunlight determines the quantity of electricity produced from the solar energy plant. The national solar radiation database information from prediction estimation of NASA on global energy resources of the industrial microgrid provided the yearly average radiation of 5.85 kWh/m<sup>2</sup>/day for Ko-Kut island coordinates (lat 11<sup>o</sup> 39'N long 102<sup>o</sup> 32'E). The highest monthly radiation occurred in october: 6.080 kwh.m<sup>-2</sup>.dy<sup>-1</sup> while the least insolation occurred in may: 5.680 kWh.m<sup>-2</sup>.dy<sup>-1</sup> from fig. 8.

The output power of solar energy plant with respect to the effect in temperature is given in equation 5.

$$SEP_{Rxa}(t) = R_{Rxa} \times D_{Rxa} \times \left(\frac{G_{Rxa}(t)}{G_{stc}}\right) \times [1 + \alpha_{Rxa} \times (T_{Rxa}(t) - T_{stc})] \quad (5)$$

The overall power generated by the number of solar-max 500 RXA modules at any given period (t) is expressed below:

$$P_{Rxa}(t) = N_{Rxa} \times SEP_{Rxa}(t) \quad (6)$$

SEP<sub>Rxa</sub>(t) = output power generated by the solar-max PVs module for a given period (t) in kW

R<sub>Rxa</sub> = Rated capacity of the solar energy plant = 500 kW

D<sub>Rxa</sub> = Solar panel's derating factor = 0.96 or 96 %

G<sub>Rxa</sub>(t) = Solar insolation penetration on the panel of the solar photovoltaic (kWm<sup>-2</sup>)

G<sub>stc</sub> = Solar insolation incidence on the panel of the solar photovoltaic at standard test condition = 1.0 × 10<sup>3</sup> Wm<sup>-2</sup>

α<sub>Rxa</sub> = Solar PV's power temperature coefficient = -0.410 %.<sup>o</sup>C<sup>-1</sup>

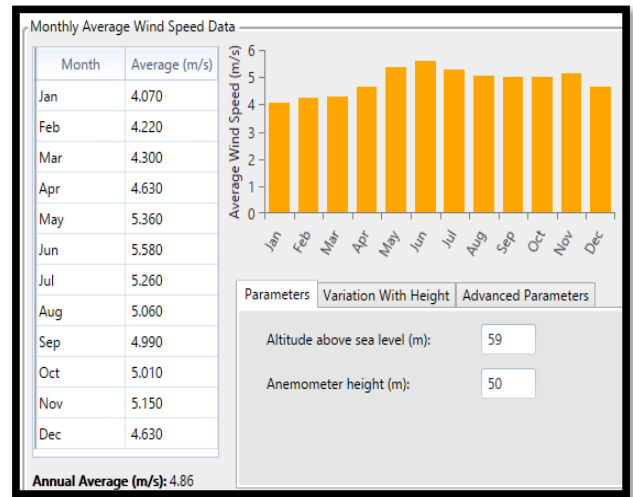


FIGURE 9. Annual and monthly average wind speed on Ko-Kut Island [61].

T<sub>Rxa</sub>(t) = Nominal solar panel's operating cell temperature = 45 <sup>o</sup>C

T<sub>stc</sub> = Solar panel's temperature at standard test condition = 25 <sup>o</sup>C

P<sub>Rxa</sub>(t) = Total Power produced from the solar energy panel in kW

N<sub>Rxa</sub> = Solar PV module's number [33].

Lifetime operation of the Solar-max PV = 25 years with respect to the solar max module lifetime.

## 2) WIND GENERATOR SYSTEM MODELING

The maximum energy/power flow production from a fixed (hub) height (m) of the generator (wind power) at any speed of the generating wind flow can be mathematically expressed below:

$$V_{ws} = V_{ws\ ref} \times \left(\frac{H_a}{H_n}\right)^\beta \quad (7)$$

V<sub>ws</sub> = wind's speed in metre/sec,

V<sub>wsref</sub> = speed of the wind at reference height in metre/sec

H<sub>a</sub> = hub's height in meters,

H<sub>n</sub> = hub height's reference in meters,

β = hellman's exponent or power-law's exponent = 0.14.

From the curve of the wind plant's model in Fig.10, it is obvious that the Ko-Kut district possesses a high wind speed which ranges from 4.070 - 5.580 m/s at a hub height of 50 m when the monthly record of the mean (average wind) speed was taken into consideration with a yearly average speed of 4.860 m/s from Fig.9 [61].

As the hub's height vary, the wind's velocity and output power generated from the turbine plant also varies.

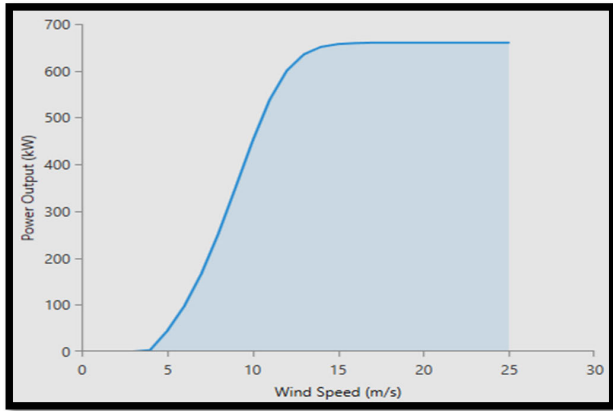


FIGURE 10. Power curve for wind generator (turbine) [62].

Where

$$\beta = [(0.37 - (0.088 \times \frac{\text{Log}_e^{v_{wsref}}}{(1 - 0.0880 \times \text{Log}_e^{(\frac{H_p}{10})})})] \quad (8)$$

The production of power from the wind energy turbine plant can be expressed below:

$$P_{opp} = 0.50 \times \rho d \times A_p \times C_{ps} \times [V_{ws}]^3 \quad (9)$$

$P_{opp}$  = wind generator (turbine) output power production (kW)

$\rho d$  = air flow pressure's density in  $\text{kg} \cdot \text{m}^{-3}$

$A_p$  = wind turbine's sweep area ( $\text{m}^2$ )

$C_{ps}$  = wind turbine's coefficient (dimensionless)

$V_{ws}$  = Wind's linear speed (m/s) [63].

The  $v_{cutin}$  and  $v_{cutout}$  speed are 4.0 and 25.0 m/s from the wind energy turbine power characteristic curve after simulation from Fig. 10, respectively.

The boundary equation relates the cutting in speed, rated wind-speed, and cutting out speed mathematically. The output power production from the wind power turbine model when its wind turbine velocity varies is mathematically expressed below.

$$V_{cutin}(t_s) < V_{ws}(t_s) < V_{Ctto}(t_s) \quad (10)$$

$$P_{opp}(t_s) = 0, \quad \text{if } V_{ws}(t_s) \leq V_{cutin}(t) \text{ or } V_{ws}(t_s) \geq V_{Ctto}(t_s) \quad (11)$$

$$P_{opp}(t_s) = P_{rae}(t_s), \quad \text{if } V_{rae}(t_s) < V_{ws}(t_s) \leq V_{Ctto}(t_s) \quad (12)$$

$$P_{opp}(t_s) = P_{rae}(t_s) \times \left[ \frac{(V_{ws}(t_s) - V_{cutin}(t_s))}{(V_{rae}(t_s) - V_{cutin}(t_s))} \right] \quad (13)$$

if  $V_{cutin}(t_s) < V_{ws}(t_s) < V_{rae}(t_s)$

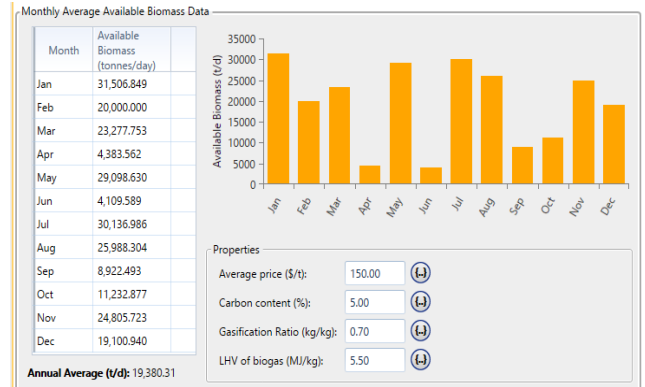


FIGURE 11. Annual average and monthly available biomass resources [64].

$P_{opp}(t_s)$  = wind energy turbine's output power production (kW)

$P_{rae}(t_s)$  = wind energy turbine's rated power in kW

$V_{ws}(t_s)$  = wind energy turbine's speed (m/s)

$V_{Ctin}(t_s)$  = wind energy turbine cut-in speed = 4 m/s

$V_{Ctto}(t_s)$  = wind generator's (turbine) cut-out speed = 25 m/s

$V_{rae}(t_s)$  = wind generator's (turbine) rated speed (m/s) [33].

The hub height options from the vestas' wind system manufacturer are 40 m, 45 m, 50 m, and 55 m. A hub height magnitude of 50 m was chosen from the schematic design of the hybrid energy control network.

### 3) BIOGAS POWER SYSTEM MODEL

The biogas power plant's rated capacity of 500 kW comprises of a combustion reaction chamber, heat regulator at the output from air supply (an inlet of air), hopper: storage of fuel, and combustion reaction chamber producing gases for outlet channeling. This gasifier (biomass generator) system converts dried biomass resources (feedstock) to mixture of gases through heating (thermal) process known as a gas turbine running operation under internal burning system (combustion). The biogas fuel was produced from the mechanical (pretreatment section: hand sorting, hopper, drum screening, magnetic separation) and chemical treatment (hydrolysis, dewatering, fermentation, and reaction from anaerobic digestion) of municipal solid wastes (rubber and leather, paper, garden wastes, food scrap, plastics, metals, textiles, leaves and woods) of 19,380.31 tonnes/day yearly mean production of biomass resources from Fig. 11 in relation to Ko-Kut Island potential resources.

The output energy production ( $E_{DBGG}(t)$ ) from the down-draft biomass gasifier-biogas generator at every hour is expressed mathematically below.

$$E_{BGP}(t) = \left[ \frac{(Q_{BGP} \times M_{BGP} \times \eta_{BGP} \times 1000)}{(860 \times 365 \times T_{BGP})} \right] \quad (14)$$

$Q_{BGP}$  = quantities of biomass resources in tonnes/day  
 $M_{BGP}$  = biomass' calorific value in megajoules/tonne =  $5500 \times 10^6$  Joules/tonne = 5500 MJ/tonne  
 $\eta_{BGP}$  = biogas power plant system's efficiency in %  
 $T_{BGP}$  = operating period of the biogas plant system on daily basis (hours) [63]

The annual mean quantity of biomass potential in Ko Kut Island,  $Q_{KKI} = 19,380.31$  tonnes/day.

#### 4) BATTERIES (VRFB, ZNBR, NAS, AND LI-ION)

The excess electric energy production from the hybrid micro-grid (DC and AC buses) network system was fed to the deferrable load, high frequency flywheel energy system and batteries for storage application after the main energy sources (solar PVsc, grid energy network, and wind energy plants) have served the primary load fully. The excess electricity stored in the batteries and flywheel will serve as emergency against capacity shortage from the main energy sources to avoid power interruption between the power sources and load. The high-energy rotational flywheel motor function as a generator and motor (power supply and energy storage sources).

The capacity of the charging batteries will occur,

$$\text{if } en_{dc/ac}(t_s) > en_{load}(t_s)$$

$$en_{bttts}(t_s) = en_{bttts}(t_s - 1) + [en_{xcess}(t_s) \times \eta_{bttts} \times \eta_{pcr}] \quad (15)$$

$$en_{xcess}(t_s) = [en_{ac}(t_s) + en_{dc}(t_s) \times \eta_{pcr}] - en_{load}(t_s) \quad (16)$$

$en_{dc/ac}(t_s)$  = direct and alternating currents energy sources producing energy at a stated time,  $t_s$  (kwh)  
 $en_{load}(t_s)$  = energy consumed by the primary (ac) load at a stated time,  $t_s$  (kwh)  
 $en_{bttts}(t_s)$  = batteries' present energy level at a particular time,  $t_s$  (kWh)  
 $en_{bttts}(t_s-1)$  = batteries' existing energy level at a stated preceding time,  $t_s-1$  (kWh)  
 $en_{xcess}(t_s)$  = direct and alternating current sources producing excess energy at a given time,  $t_s$  (kWh)  
 $en_{ac}(t_s)$  = alternating current sources generating energy at a given time,  $t_s$  (kWh)  
 $en_{dc}(t_s)$  = direct current sources generating energy at a given time,  $t_s$  (kWh)  
 $\eta_{bttts}$  = charging batteries' efficiency (%)  
 $\eta_{pcr}$  = power (bi-directional) converter's efficiency (%).

The capacity of the storage system (batteries) occurs,

$$\text{If } EN_{DC/AC}(t_s) < EN_{load}(t_s)$$

$$EN_{bttts}(t_s) = (1 - \beta) \times EN_{bttts}(t_s - 1) - \left[ \frac{EN_{xcessload}(t_s)}{(\eta_{bttts-discr} \times \eta_{pcr})} \right] \quad (17)$$

$$EN_{xcessload}(t_s) = EN_{ACload}(t_s) - [EN_{AC}(t_s) + EN_{DC}(t_s) \times \eta_{pcr}] \quad (18)$$

$EN_{xcessload}(t_s)$  = extra energy needed to serve the primary (AC) load at a stated time,  $t_s$  (kWh)  
 $\beta$  = rate at which the batteries discharge automatically per hour  
 $\eta_{bttts-discr}$  = efficiency of the discharging batteries (%) [63].

#### 5) HIGH FREQUENCY-ENERGY ROTATING MASS FLYWHEEL

The flywheel is a compact rotating mass electromechanical storage device that receives a standby 12 kW parasitic load loss from the hybrid energy sources and versatile based grid stabilizing generator in energy production with an operating reserve capacity of 458 kW, stabilizing the power system network against voltage/frequency fluctuations, assisting the network by charging the batteries, improving the batteries' lifespan, and preventing over-charging and over-dis-charging stress from the batteries. The parallel connection of the flywheel system with the solar PVsc, wind turbine, utility grid, and biogas generator will dampen the effect of maximum demand (load) when the solar PVsc and wind turbine experiences low energy production than the demand capacity. Thereby, making the flywheel-grid stabilizer system to consume larger amount of electricity than the batteries. This will reduce the batteries input and output electric flow. In addition, the inertia property of the flywheel system opposes and moderate fluctuations from the solar PVsc, wind turbine, and utility grid to prevent unstable current from damaging the batteries. If the flywheel is connected in parallel with the batteries, it (flywheel) will reduce the peak energy demand by improving the batteries life cycle and cyclic stress, thereby, making the batteries to accumulate or deliver a steady slow quantity of energy variation. The flywheel system operation also enables peak shaving extension with the grid system to hinder exchanging strong oscillatory energy profile.

The energy ( $E_{nerg-fess}$ ) stored by the electromechanical device (flywheel) in the hybrid energy network is given by the expression below.

$$E_{nerg-fess} = 1/2 \times I_{pfess} \times \omega_p^2 \quad (19)$$

$I_{pfess}$  = flywheel's moment of inertia in  $kgm^2$   
 $\omega_p$  = flywheel's angular velocity in rad/sec [60].

#### 6) POWER GTP519S 900 kW, 700 V DC BI-DIRECTIONAL CONVERTER

The 3-phase 900 kW, 700 V D.C is a bi-directional converter, grid following charge controller. The utility grid network, hybrid generators, and energy reserve systems are connected to the 3-phase bi-directional converter to operate in a rectification mode for the AC power sources (biomass

gasifier, utility grid, vestas wind turbine, solar max with dedicated inverter, and flywheel) and inversion mode for the DC (batteries) sources. The rated efficiency and power of the bidirectional energy conversion system is given as.

$$\eta_{\text{power-bdconv}} = \left[ \frac{\text{output power(kW)}}{\text{input power(kW)}} \right] \quad (20)$$

$$P_{\text{-Leon-BDC}}(t) \times 100\% = P_{\text{nwr-in}}(t) \times \eta_{\text{power-bdconv}} \quad (21)$$

$H_{\text{Power-bdconv}}$  = efficiency of the bi-directional power converter in %

$P_{\text{-Leon-BDC}}$  = output power flow rating of the bi-directional converter (kW) [33], [66]

$P_{\text{nwr-in}}(t)$  = input power (kW) flow transferred to the power converter system.

The econometric and technical characteristic values of the integrated hybrid energy network are tabulated in Table 5 under the appendix section.

### III. ECONOMIC ESTIMATION OF THE HYBRID ENERGY NETWORK

The application of HOMER power grid software in optimizing the schematic designed hybrid energy network provided a comprehensive econometric estimation summary in terms of the net present/initial capital/operational/maintenance/levelized energy cost values including the most convenient strategy for managing multiple energy sources efficiently and the most preferred energy source as a switching option when a multiple control strategy algorithm was introduced into the hybrid energy system.

$$A_{\text{cc}} = \text{NPV}_{\text{cc}} \times I_{\text{FC}} \times \left[ \frac{(1+I_{\text{FC}})^k}{(1+I_{\text{FC}})^k - 1} \right] \quad (22)$$

where

$$\text{NPV}_{\text{cc}} = \sum_{t_i=0}^k \frac{\text{NCF}_{t_i}}{(1 + I_{\text{FC}})^{t_i}} - C_{\text{Inc}} \quad (23)$$

$A_{\text{cc}}$  = annuity (in dollars)

$\text{NPV}_{\text{cc}}$  = net present value (in dollars)

$I_{\text{FC}}$  = interest of fictitious (in %)

$K$  = period of planning (in years)

$C_{\text{Inc}}$  = overall cost of investment (in dollars)

$\text{NCF}_{t_i}$  = net cash flow at a period  $t_i$  (in dollars)

$t_i$  = cash flow period (in years).

$$\text{Annuity factor, } A_{\text{ff}} = I_{\text{FC}} \times \left[ \frac{(1 + I_{\text{FC}})^k}{(1 + I_{\text{FC}})^k - 1} \right] \quad (24)$$

The product of net present value ( $\text{NPV}_{\text{cc}}$ ) with annuity factor ( $A_{\text{ff}}$ ) gives the annuity value in dollars according to the currency applied to the software design. To evaluate or calculate the  $\text{NPV}_{\text{cc}}$  of the hybrid energy network, net cash flow at a given period  $t_i$  was considered in terms of payment series during the period of planning,  $k$ .

$$L.C.O.Es = \left[ \frac{A_{\text{nt}}}{(E_{\text{nerdem}})} \right] \quad (25)$$

L.C.O.Es = Levelized cost of energy in \$/kWh

$A_{\text{nt}}$  = overall annuity in dollars

$E_{\text{nerdem}}$  = energy demand in kWh

For an energy project to be economically feasible, it must rely on the total cost of power generated. Levelized energy cost, L.C.O.E is the overall expense from each power (generating) source expressed as a fraction of the generated volume of electricity over the life span of the hybrid energy network project. The percentage of renewable energy (inflow) sources from the overall unified energy network is expressed as a renewable fraction.

$$\text{RF}_r (\%) = \left( 1 - \frac{\sum_{t=1}^n P_{\text{NRS}}}{\sum_{t=1}^n P_{\text{gen}}} \right) \times 100 \% \quad (26)$$

$\sum P_{\text{NRS}}$  = total power generated from nonrenewable energy sources in kW

$\sum P_{\text{gen}}$  = total power generated from the hybrid network system in kW [65].

### IV. TECHNICAL OPERATION AND ECONOMIC ANALYSIS OF THE INTEGRATED ENERGY NETWORK

The control systems (combined dispatch, loads following, and cycles charging) was designed with the hybrid energy network to provide proper control, effective monitoring, and central management for the generators (power sources), storage units, and loads, respectively. The combined dispatch embodies the cycle charging and load monitoring controllers by making final decision on the most preferable option between the two sub-control systems (cycle charging and load following) for the energy system architectures. From the entire energy network, the load-following or cycle charging controller could be the appropriate choice designated by the combined dispatch for effective and efficient energy control over the grid system architectural modes.

#### A. GRID-CONNECTED HYBRID ENERGY SYSTEM-POWER RESERVE NETWORK

The modelled hybrid energy system architectural design (biomass gasifier generator/wind V47 turbine plant/Solar max PVsc/Flywheel/VRXFB-NaS-Li<sup>+</sup>-ZnBr batteries) was connected to the utility grid network. Optimization results was obtained from 4 different architectures of the hybrid power network relating their economic properties (net present costs, electric energy cost, operating cost, maintenance cost, replacement cost, fuel costs, and initial capital investment), and operations (total fuel consumption, annual energy production, and energy system fraction) within the Ko-kut Island atmosphere.

A control system unit for the grid-connected hybrid energy network adopted the cycle charging strategy as the best option for this architectural design, this dispatch strategy allows the power generators to feed the load at its full output (power) capacity. The excess generated electricity will flow towards the lower priority objectives in a decreasing order by serving

the deferrable loads, charging the energy reserve systems: flywheel/batteries storage systems (if not fully charged). The cycle charging strategy monitors the set-point charging state of the batteries by preventing over charging of the batteries. As the batteries attain their maximum level of charging state (100 %), the cycle charging controller disengages the batteries from the supply source. When the load and storage units are fully met, the excess production of electricity left will be sold to the utility grid network. The load monitoring or load following energy strategy triggers the utility grid and flywheel system (AC generator) to supply the appropriate power to balance the load only. While the biogas, wind V47, and solar PVsc generators produce enough electricity to power the deferrable load and store charges on the hybrid batteries. They (biogas, wind V47, and solar PVsc generators) can also boost the hybrid energy network capacity by selling their excess generated electricity to the utility grid after charging the batteries to their respective maximum storage capacity. The renewable generators (biogas, wind V47, and solar PVsc) and grid system are capable of energizing the flywheel system because the electromechanical system (flywheel) operates in two different dimensions (as an AC generator and AC motor with dedicated inverter integration).

After simulating the grid-renewable generating system, the solar/wind/biomass gasifier/VRFB battery/flywheel/grid and solar/wind/biomass gasifier/flywheel/Lithium-ion battery/grid system architectures sold more electric energy to the utility grid than their respective power purchase from the grid network with a cheaper annual energy cost as charges.

The two system architectures (each) produced the same value of annual energy purchase (476,916 kWh/yr) and annual energy sales (568,553 kWh/yr) to the grid system with an annual energy charge of \$4,581.86. Each system architecture purchased the highest (57,017 kWh) and lowest (21,199 kWh) value of electricity in the month of September and December. Another record from the simulation result indicates the energy systems had the highest (83,641 kWh) and lowest (17,834 kWh) sales of electricity in December and October. Each energy system experienced the highest (468 kW) and least (250 kW) peak load demand in August and December with an annual average peak demand of 468 kW. The significance of Li-ion and VRFB energy system architectures has shown similar efficient operation in their grid sales activity over their grid purchase activity. Both systems are economically and technically efficient over the grid network service and load, respectively. Hence, both energy systems are profitable and reliable, thereby, demonstrating their supporting capacities as an edge over the grid network and variable peak energy demand during the year. The batteries (Li-ion and VRFB) possess some properties in common such as medium duration service application (load deviation management and fixing power capacity shortage) and long duration service usage (extension of power system connection, power flow, and reliability measure). The negative value of the annual net energy purchase (-91,637 kWh)

between the utility grid and hybrid Li-ion-VRFB-renewable generators indicate the dominant economic force of the hybrid renewable generators and storage systems over the utility grid operation. The network operation purchased more energy from the grid in May (45,736 kWh), August (52,030 kWh), September (57,017 kWh), and October (53,306 kWh) when the microgrid productivity was low. While the remaining period (months) recorded higher sales of electricity from the microgrid network transported to the grid system. When the utility grid energy is low, the microgrid network is at a greater advantage to sell more energy to the utility grid provided its (microgrid) productivity is higher than the grid production value.

The graphical information from the two-hybridized energy systems' design from Fig.13 and Fig.14 depicts the biomass gasifier plant as a secondary power source that only operates when the solar PVsc/Vestas-wind plant/grid systems are out of service, thereby functioning as an energy backup source. The energy system configuration possesses 75 % of renewable fraction with 0.0025 % of annual excess electricity value (51.2 kWh/yr), and the annual energy consumption (2,015,232 kWh/yr) is slightly higher than its production (2,015,100 kWh/yr) due to 28.2 % of energy sold (568,553 kWh/yr) to the grid network. The wind generator (turbine) plant produced the largest annual energy share (46.6%: 938,364 kWh/yr) than the grid share and other sustainable power sources, respectively.

The significance of Zn-Br and Na-S energy system architectures from Fig.15 portrays its economic disadvantage against the grid network service. Clearly depicting the technical efficiency of the network in fulfilling the load requirement but not profitable economically. The microgrid network productivity (energy sold) was lower than the utility grid productivity (energy purchased). Hence, the grid system is at an economic advantage over the microgrid network when the annual net energy purchase is positive (245,139 kWh). The solar PVsc/wind/biomass/ZnBr and NaS batteries/flywheel/grid/converter energy system configuration from Fig.16 tends to generate lower annual energy (1,863,923 kWh/yr) with the wind turbine plant contributing the major (50.3 %) energy supply from the hybrid power sources. The renewable fraction of the configuration depreciated to 62.3 % with lower annual energy consumption (1,864,347 kWh/yr) and excess annual electric energy (131 kWh/yr) than the solar PVsc/wind turbine/biomass gasifier/Li<sup>+</sup>-VRFB/grid/converter energy system configuration (51.2 kWh/yr) from Fig.14. The energy system from Fig.16 purchased more energy (35.6 %) from the grid system than what was sold (22.4 %) towards it (grid network), indicating a high annual positive net energy purchase (662,808 - 417,669 = 245,139 kWh/yr) than the energy system from Fig.13 (solar PVsc/wind turbine/biomass gasifier/Li<sup>+</sup>-VRFB/grid/converter) with an annual negative net energy (476,916 - 568,553) purchase of -91,637 kWh/yr. The assessed energy system from Fig.13 is highly profitable and economically stable than the energy system from Fig.16



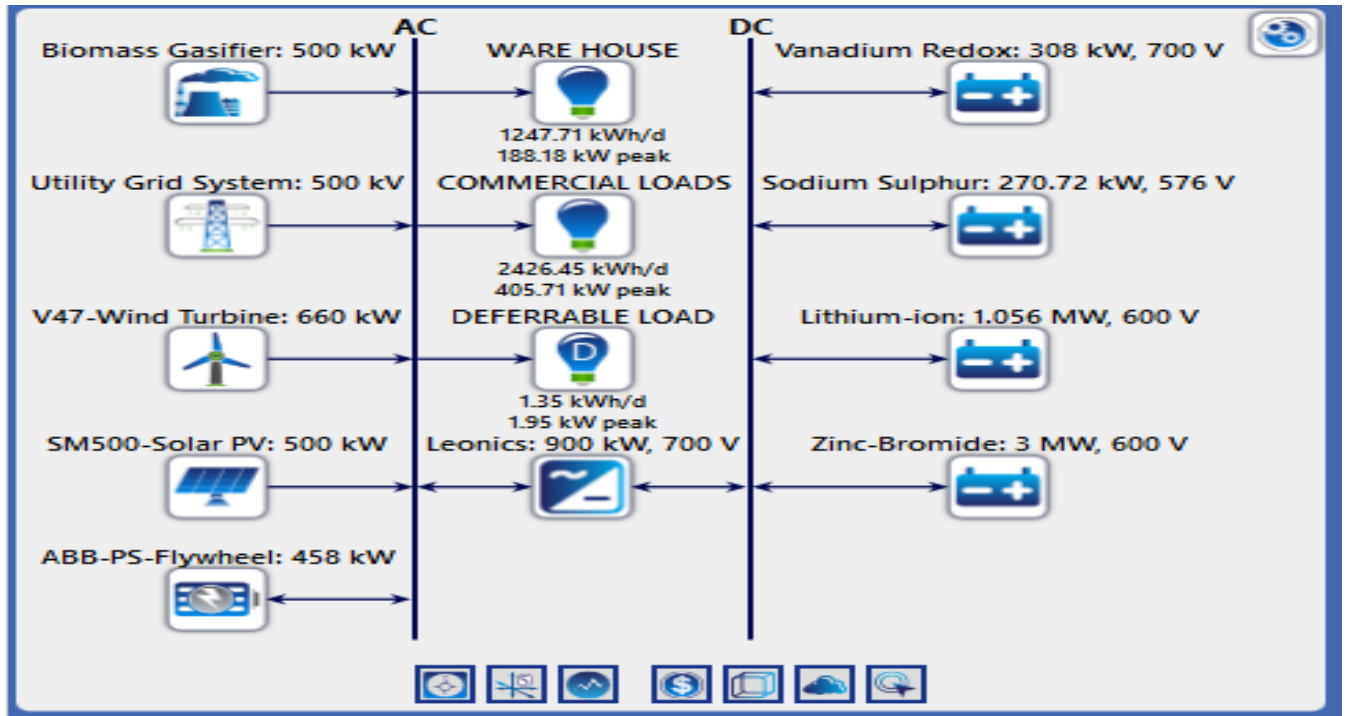


FIGURE 12. Grid integrated hybrid energy network and control systems simulation.

Month	Energy Purchased (kWh)	Energy Sold (kWh)	Net Energy Purchased (kWh)	Peak Load (kW)	Energy Charge \$	Demand Charge \$
January	26,301	49,674	-23,373	288	\$0	\$0
February	25,561	47,789	-22,228	293	\$0	\$0
March	31,976	58,596	-26,620	294	\$0	\$0
April	36,473	41,773	-5,299	306	\$0	\$0
May	45,736	36,538	9,198	372	\$0	\$0
June	51,630	56,764	-5,134	465	\$0	\$0
July	46,282	51,789	-5,507	431	\$0	\$0
August	52,030	49,834	2,196	468	\$0	\$0
September	57,017	19,273	37,743	441	\$0	\$0
October	53,306	17,834	35,472	383	\$0	\$0
November	29,405	55,049	-25,643	325	\$0	\$0
December	21,199	83,641	-62,442	250	\$0	\$0
Annual	476,916	568,553	-91,637	468	(\$4,581.86)	\$0

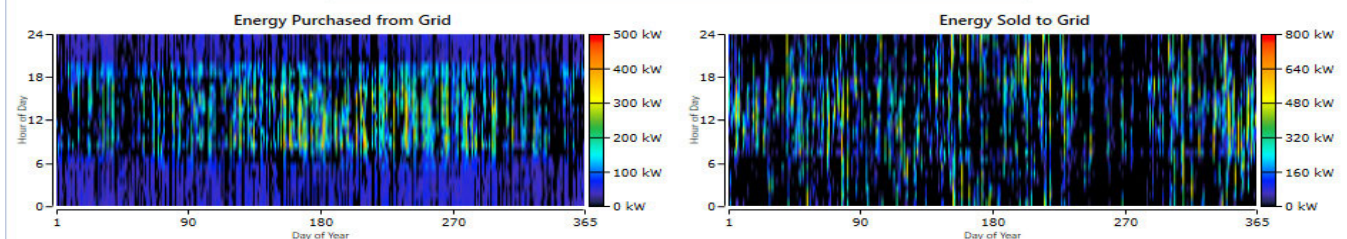


FIGURE 13. Grid rate schedule of solar/wind/biomass/Li<sup>+</sup>-VRFB/flywheel/grid/converter configurations.

and other grid-connected hybrid energy system architectures. The similarities in the properties of Zn-Br ion and Na-S batteries concentrate on their load deviation management and fixing power capacity shortage applications in supporting the utility grid network.

The combined dispatch strategy (central control system) assign the appropriate control strategy for the hybrid energy

network by selecting either cycle charging or load following control system during electrification, energization, energy utilization, and economic management of the entire network configuration during operation. The control strategy that was assigned autonomously by the combined dispatch controller to the individual hybrid generating network configuration is tabulated in Table 1.

Production	kWh/yr	%	Consumption	kWh/yr	%	Quantity	kWh/yr	%
SolarMax 500RX A with Generic PV	599,820	29.8	AC Primary Load	1,341,066	66.5	Excess Electricity	51.2	0.00250
Generic Biogas Genset (size-your-own)	0	0	DC Primary Load	0	0	Unmet Electric Load	0	0
Vestas V47 [660kW]	938,364	46.6	Deferrable Load	493	0.0244	Capacity Shortage	0	0
Grid Purchases	476,916	23.7	Grid Sales	568,553	28.2			
Total	2,015,100	100	Total	2,015,232	100			

Quantity	Value	Units
Renewable Fraction	75.0	%
Max. Renew. Penetration	100	%

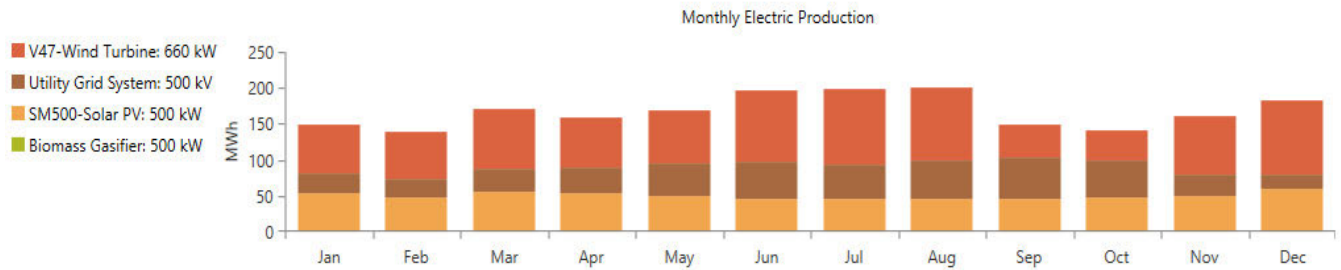


FIGURE 14. Electricity production of solar/wind/biomass/Li+ -VRFB/flywheel/grid/converter.

Month	Energy Purchased (kWh)	Energy Sold (kWh)	Net Energy Purchased (kWh)	Peak Load (kW)	Energy Charge \$	Demand Charge \$
January	39,703	32,470	7,233	303	\$0	\$0
February	38,114	33,832	4,282	318	\$0	\$0
March	46,020	41,762	4,258	334	\$0	\$0
April	53,673	29,017	24,656	355	\$0	\$0
May	64,460	26,945	37,515	385	\$0	\$0
June	67,889	47,620	20,269	486	\$0	\$0
July	62,913	42,292	20,621	477	\$0	\$0
August	66,837	38,569	28,268	488	\$0	\$0
September	76,635	13,173	63,462	458	\$0	\$0
October	72,163	10,481	61,682	390	\$0	\$0
November	43,513	41,092	2,420	345	\$0	\$0
December	30,887	60,415	-29,528	273	\$0	\$0
Annual	662,808	417,669	245,139	488	\$36,770.92	\$0

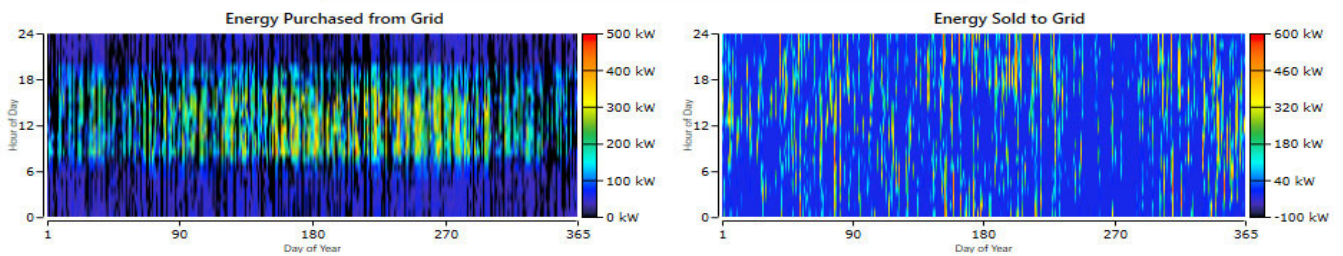


FIGURE 15. Grid rate schedule of solar/wind/biomass/flywheel/ZnBr/Na-S/grid/converter.

**B. ENVIRONMENTAL EMISSION-COST SUMMARY OF PROPOSED INTEGRATED HYBRID ENERGY NETWORK**

The grid connected-hybrid energy network consists of 4 different system architectures from the simulation design. A tabulated result for the simulation process from Table 2 shows their configurations, quantity of gas emission, and cost summaries. The configuration of solar PVsc/wind/bio-gasifier/NaS/flywheel/Leonics converter/grid had the highest cost of operation (\$107,249.40), second to the highest net present value (\$2,948,606), and the highest levelized energy

cost (\$0.1297) as compared to other architectures while the solar PVc/wind/bio-gasifier/VRFB/flywheel/grid system had the least operating cost (\$58,830.93), least net present cost (\$2,502,038.00) and the least levelized energy cost (\$0.1013/kWh) as the most affordable hybrid energy system, economically, with a moderate annual gas emission of 303,357 kg/yr. Considering the most efficient, sustainable, and reliable network in terms of power delivery/consumption, excess energy, and grid sales, preference was given to the hybrid configuration of solar PVc/wind/bio-gasifier/

Production	kWh/yr	%
SolarMax 500RX A with Generic PV	262,751	14.1
Generic Biogas Genset (size-your-own)	0	0
Vestas V47 [660kW]	938,364	50.3
Grid Purchases	662,808	35.6
Total	1,863,923	100

Consumption	kWh/yr	%
AC Primary Load	1,341,066	71.9
DC Primary Load	0	0
Deferrable Load	492	0.0264
Grid Sales	417,669	22.4
Total	1,864,347	100

Quantity	kWh/yr	%
Excess Electricity	131	0.00700
Unmet Electric Load	0	0
Capacity Shortage	0	0

Quantity	Value	Units
Renewable Fraction	62.3	%
Max. Renew. Penetration	100	%

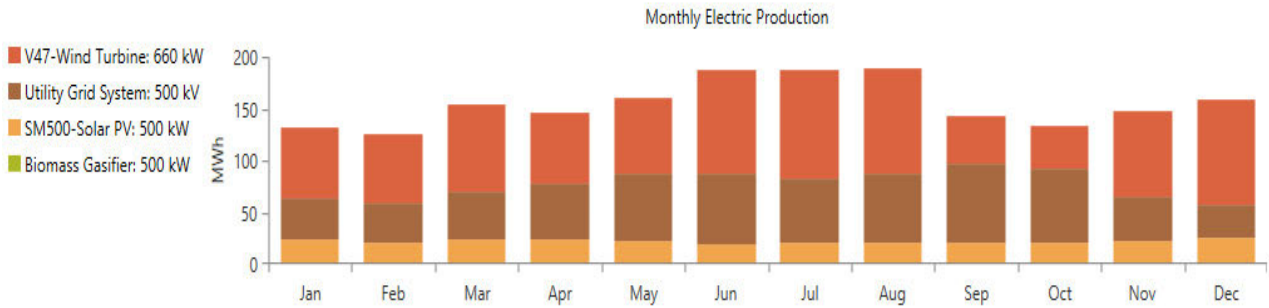


FIGURE 16. Electricity production of solar/wind/biomass/ZnBr-NaS/flywheel/grid/converter.

TABLE 1. Energy system architecture and control strategy.

Hybrid system configuration	Control dispatch strategy
Solar/wind/biomass gasifier/VRFB/flywheel/grid/converter	Cycle charging
Solar/wind/biomass gasifier/flywheel/ZnBr/grid/converter	Load following
Solar/wind/biomass gasifier/flywheel/NaS/grid/converter	Load following
Solar/wind/biomass gasifier/flywheel/Li <sup>+</sup> /grid/converter	Cycle charging

Li<sup>+</sup>-VRFB/converter/grid network that both generated the same highest annual energy of 2,015,100 kWh/yr and the least excess energy (51.2 kWh/yr) with a peak renewable contribution of 100 % from Fig.14 after all necessary conditions between the energy production and consumption were fulfilled.

The economics and technical feasibility of the hybrid energy network are represented with their waveform from Fig.17 and Fig.18, depicting their (hybrid generators' network) reliability measure in satisfying the demand, making much profit from investment and the hybrid storage potential capacity support at full measure in generating more electricity than the grid system supply in Ko-Kut Island, Thailand.

The grid connected to the hybrid generators without batteries produced a return of investment (19 %) with an internal return rate of 22 %. The grid-connected system has a pay-back (4.4 years) period after investment. The cost summary

TABLE 2. Gas emission-cost evaluation of the hybrid energy-grid network.

Proposed system architecture	Gases	Quantities (kg/year)	Cost summary (\$)	
Solar/wind/biomass gasifier/VRFB/flywheel/converter/grid	CO <sub>2</sub>	301,411	Total N.P.C: \$2,502,038	
	CO	0	Levelized C.O.E: \$0.1013	
	C <sub>x</sub> H <sub>y</sub>	0	Operating cost: \$58,830.93	
	Particles	0	Total N.P.C: \$3,126,035	
	SO <sub>2</sub>	1,307	Levelized C.O.E: \$0.1266	
Solar/wind/biomass gasifier/Li <sup>+</sup> /flywheel/converter/grid	NO <sub>x</sub>	639	Operating cost: \$76,158.09	
	Solar/wind/biomass gasifier/ZnBr/flywheel/converter/grid	CO <sub>2</sub>	418,895	Total N.P.C: \$2,899,864
		CO	0	Levelized C.O.E: \$0.1275
		C <sub>x</sub> H <sub>y</sub>	0	Operating cost: \$101,931.9
		Particles	0	0
SO <sub>2</sub>		1816	Total N.P.C: \$2,948,606	
Solar/wind/biomass gasifier/NaS/flywheel/converter/grid	NO <sub>x</sub>	888	Levelized C.O.E: \$0.1297	
			Operating cost: \$107,249.4	
			0	

for the base case and proposed grid connected network can be deduced from the values of the grid mode at a lower

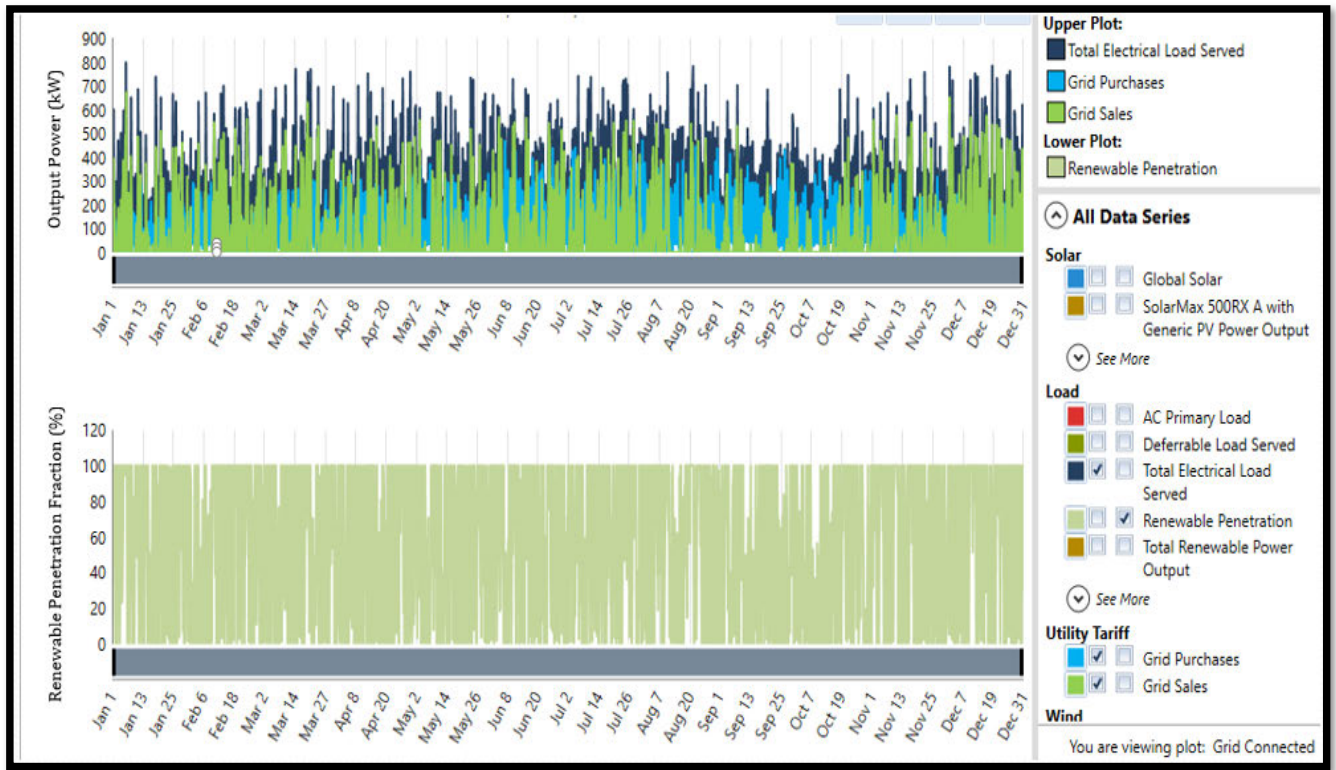


FIGURE 17. Annual cash flow of power production and renewable penetration.

cost except for the initial capital cost (base case: \$304,000) because of complexity in the facilities involved in relation to Fig.18. As the project lifespan advances (0 to 25 years), the annual worth of the grid connected proposed system drops in value from \$1,045,641.79 to \$134,001.48 with its base case (\$304,000 to \$70,289.14) value during this life period. At 5.2 years projection of the grid-connected hybrid energy system, its cumulative nominal cash flow (\$1,300,000) at the given period (5.2 years) from the graph marks the point of intersection between the lowest cost system and base case scenario, signifying a balanced point of economic force between the two financial factors from the grid connected microgrid system.

Table 3 has given the incurred annual net value of benefit-cost (annual worth) from each hybrid system design with respect to their present cash value in equivalent amount to their future received payment (present worth). The present worth value of solar/wind/biomass gasifier/flywheel/Li<sup>+</sup>/grid architecture produced the least (\$69,048) amount with the least investment return (4.0 %) and highest payback period (11.25 years) in comparison with solar/wind/biomass gasifier/VRXFB/flywheel/grid architecture having the highest present worth value (\$693,045), highest investment return (7.5 %) and the highest internal return rate (10.6 %) with the lowest payback period (8.57 years). In the aspect of business investment from the various architectural designs, the solar/wind/biomass gasifier/VRXFB/flywheel/grid network is the best choice over the

TABLE 3. Economic comparison of energy system architectures on grid connection.

Proposed system architecture	Present worth (\$)	Yearly worth (\$)	Investment return (%)	Internal return rate (%)	Payback period (years)	Payback discount (years)
Solar/wind/bio-gasifier/VRXFB/flywheel/grid/converter	693,045	53,610	7.5	10.6	8.57	12.31
Solar/wind/bio-gasifier/flywheel/ZnBr/grid/converter	295,219	228,37	5.6	8.2	10.42	16.49
Solar/wind/bio-gasifier/flywheel/NaS/grid/converter	246,476	19,066	5.3	7.9	10.26	16.06
Solar/wind/bio-gasifier/flywheel/Li <sup>+</sup> /grid/converter	69,048	5,341	4.0	6.3	11.25	24.43

other hybrid generators network architecture when relating them with payback/discount periods, investment return, and internal return rate from Table 3, respectively.

Data obtained from Table 4 after simulating the various grid-connected hybrid generators configuration has proven that the hybrid architecture of solar PVsc, wind generator, biomass gasifier, flywheel/Li<sup>+</sup>, VRXFB batteries/grid/converter system produced the best and the same technical (energy) efficiencies with a considerable annual energy charge than the other configurations. The architectures

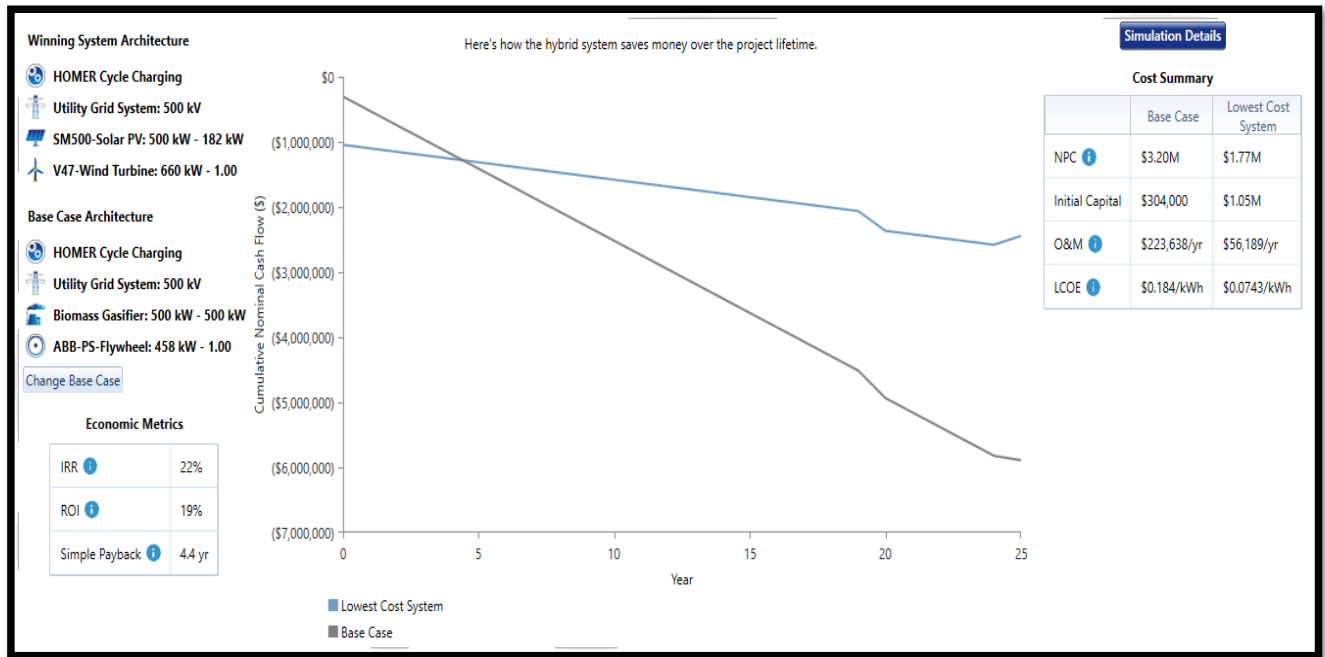


FIGURE 18. Grid connected cumulative nominal cash flow and system lifetime.

TABLE 4. Rate schedule of the hybrid power network architecture-grid connection.

Hybrid Power Network Architecture	Yearly Energy Purchase (kWh/yr.)	Yearly Energy Sales (kWh/yr.)	Net Yearly Energy Purchase (kWh/yr.)	Annual Peak Load Demand (kW)	Yearly Energy Charge (\$)	Yearly Demand Charge (\$)
Solar/wind/biomass gasifier/grid	514,069	502,849	11,220	468	1,683.04	0
Solar/wind/biomass gasifier/VRFB-ZnBr-NaS-Li <sup>+</sup> /grid/converter	591,408	451,389	140,019	476	21,002.92	0
Solar/wind/biomass gasifier/flywheel/grid	525,660	513,393	12,262	474	1,840.05	0
Solar/wind/biomass gasifier/flywheel/ZnBr-NaS/grid/converter	662,808	417,669	245,139	488	36,770.92	0
Solar/wind/biomass gasifier/flywheel/Li <sup>+</sup> -VRFB/grid/converter	476,916	568,553	-91,637	468	4,581.86	0

of Li<sup>+</sup> and VRXFB energy systems sold more energy (568,553 kWh/yr) to the grid system than their energy purchase (476,916 kWh/yr) from the utility grid system, thereby satisfying the peak load demand (468 kW) as the least value. The simulation result (Table 4) from the scheduled operation of the hybrid power network connected to the utility grid analyzed the dynamics of the network’s flexibility under combined dispatch strategy. Thereby, enabling the stable generators (biogas and flywheel) to operate at their maximum level as a standby energy support against the unstable generators (solar PVsc and wind V47 plant: when they run below productivity in their capacity) and grid fluctuation at maximum demand. Also, the standby generators (biogas and flywheel systems) can receive additional support from the storage units (Li<sup>+</sup>, NaS, ZnBr, and VRXFB batteries) and solar PVsc/wind generators to provide economic advantage by selling excess energy to the grid system when

demand is low. This explains a contract agreement between the grid system organization and the smart grid (microgrid network) operation. When energy production from the microgrid system is not sufficient during high energy demand, grid purchases out stand grid sales but when energy production from the smart grid is sufficient, grid sales out stand grid purchases. The grid system potential can support the renewable generators and storage systems and in return obtain support from them simultaneously. The storage systems can provide energy support for one another and back up the flywheel at the same period depending on the operating potential condition of the main and standby energy sources. The batteries can go through complete isolation when fully energized by the generators and when they (grid and renewable generators) operate at their respective maximum potential capacities to feed the peak demand and sell excess energy to the network (grid) as a multi-flexible operation process of the unified

generating system with grid sales overcoming grid purchases, respectively.

## V. CONCLUSION

The economics, energy, and technical efficiencies in relation to the integrated hybrid network has been fully assessed and analyzed in accordance with their various operating system architectures. The simulation result obtained from the grid hybrid energy network has proven that not all the power system architectures was feasible economically (table 3) and technically (table 4) as detailed from the tables above. The solar/wind turbine/biomass gasifier/Li<sup>+</sup>-VRXFB/flywheel/grid system configuration from Fig.13 was assigned a cycle charging strategy as a suitable controller from the central control system. The annual energy sold (568,553 kWh) to the grid system exceeded the annual energy purchased (476,916 kWh) from the simulated grid as scheduled with a considerable annual energy charge of \$4,581.86 when compared against the grid schedule for solar/wind turbine/biomass gasifier/ZnBr-NaS/flywheel/grid/converter configuration that adopted load following control strategy having more annual energy purchased (662,808 kWh) from the grid than the annual sales (417,669 kWh) to the grid with higher annual energy charge (\$36,770.92) from Fig.15. Hence, the configuration of solar/wind turbine/biomass gasifier/Li<sup>+</sup>-VRXFB/flywheel/grid system was technically efficient than the solar/wind turbine/biomass gasifier/ZnBr-NaS/flywheel/grid system configuration. The grid schedule for the solar/wind turbine/biomass gasifier/ZnBr-NaS/flywheel/grid configuration produced lower efficiency (0.007 %) with an excess electricity of 131 kWh/yr from the annual energy (1,863,923 kWh/yr) production and 62.3 % of renewable fraction which was lesser than the solar/wind turbine/biomass gasifier/Li<sup>+</sup>-VRXFB/flywheel/grid configuration with a yearly generation of 2,015,100 kWh/yr, renewables fraction of 75 % and 0.0025 % of excess energy production (51.2 kWh/yr) from Fig.16 and Fig.14. The econometric evaluation indicated that the architecture of solar/wind/biomass gasifier/VRXFB/flywheel/grid system was the most economically feasible power network system with the highest investment return (7.5 %), internal return rate (10.6 %) and the least payback period (8.57 years) when compared against the network architectural design varieties from table 3. Showing more production in business investment and economic viability from the grid connected network in Ko-Kut Island energy system assessment. Considering the emission and cost evaluation properties of the hybrid energy-grid network configuration from table 2, it was observed that the integrated solar/wind/biomass/Li<sup>+</sup>/flywheel/grid and solar/wind/biomass/VRXFB/flywheel/grid systems both had the same and lowest emission properties as compared against the integrated ZnBr and NaS configuration network (having the same and higher emission properties than the former). Finally, the solar/wind/biomass/VRXFB/flywheel/grid had the least overall net current cost (\$2,502,038), energy cost

**TABLE 5. Economical/technical properties of integrated hybrid energy network (specification sheet of homer microgrid energy system analysis).**

Energy system (s)	Characteristics	Size (Magnitude)
Biogas energy generator	Rated capacity	500 kW, 480 V
	Capital cost	\$ 400,000
	Replacement cost	\$ 166,400
	Operational/maintenance cost	\$0.10/operation hour
	Lifespan operational service	10.0 years
	Minimum load ratio	50 %
Grid network	Capital cost	\$11,344/km
	Operational/maintenance cost	\$160 yr <sup>-1</sup> km <sup>-1</sup>
	Utility tariff	\$0.150/kWh
	Net excess grid tariff	\$0.050/kWh
	Sales' Capacity	>1MW, 500 kV
Vestas V47 Wind turbine	Rated capacity	660 kW, 690 V
	Hub height	50.0 m
	Capital cost	\$500,000
	Replacement cost	\$250,000
	Operational/maintenance cost	\$50,000
	Lifespan operational service	20 years
	Cut <sub>in</sub> Speed	4.0 m/s
Cut <sub>out</sub> Speed	25.0 m/s	
	Overall loss factor	16.0 %
Solar max 500 RX PVsc	Rated capacity	500 kW, 600 V D.C
	Temperature's coefficient	-0.41 % °C <sup>-1</sup>
	Normal operational cell's temperature	45°C
	Efficiency (at S.T.C)	17.30 %
	Capital cost	\$1,500,000
	Replacement cost	\$1,500,000
	Operational/maintenance cost	\$10 per year
	Lifespan operational service	25.0 years
	Derating factor	96 %
	Tracking control system	2 axes (vertical and horizontal)
	Dedicated converter	500 kW
	Efficiency of dedicated converter	98 %
Lifespan of dedicated converter	25.0 years	
High energetic-frequency flywheel	Parasitic load	12 kW
	Charging/discharging capacity (operational reservation)	458 kW
	Capital cost	\$300,000
	Replacement cost	\$200,000
	Operational-maintenance cost	\$4,580/year
	Minimum storage life	4.0 years
	Lifespan of operation	20.0 years
Lithium ion	Rated capacity	1 MW
	Nominal voltage value	600 V
	Nominal capacity value	4220 kWh 7030 Ah
	Cyclic efficiency	90 %
	Peak charging current	1760 A
	Peak discharging current	1760 A
	Capital cost	\$500,000
	Replacement cost	\$500,000
	Operational-maintenance	\$5000/year

**TABLE 5. (Continued.) Economical/technical properties of integrated hybrid energy network (specification sheet of homer microgrid energy system analysis).**

	cost	
	Minimum lifespan of storage system	5.0 years
	Initial Charging state	100 %
	Minimum Charging state	20.0 %
	Lifespan of operation	15.0 years
Zinc Bromide flow	Rated capacity	3 MW
	Nominal voltage value	600 V
	Nominal capacity value	1000 kWh 1670 Ah
	Cyclic efficiency	90 %
	Peak charging current	1670 A
	Peak discharging current	5000 A
	Capital cost	\$400,000
	Replacement cost	\$400,000
	Operational-maintenance cost	\$5000/year
	Minimum lifespan of storage system	5.0 years
	Initial charging state	100 %
	Lifespan of operation	30.0 years
	Minimum Charging state	20.0 %
Energy conversion (converter)	Rated capacity	900 kW
	Nominal voltage rating	700 V (D.C)
	Capital cost	\$270,000
	Replacement cost	\$270,000
	Lifespan operation	10.0 years
	Inverter's efficiency (input)	96 %
	Rectifier's efficiency (input)	96 %
	Rectifier's relative capacity	100 %
	Connection	Parallel with AC generators
Sodium Sulphur	Rated capacity	308.9 kW
	Nominal voltage	192 V
	String of 3 batteries in series connection	576 V
	Nominal capacity	3 × 1450 kWh = 4,350 kWh 3 × 7550 Ah = 22,650 Ah
	Cyclic efficiency	85 %
	Peak charging current	1200 A
	Peak discharging current	1410 A
	Capital cost	\$380,000
	Replacement cost	\$380,000
	Operational-maintenance cost	\$5000/year
	Minimum lifespan of storage system	5.0 years
	Initial charging state	100 %
	Lifespan of operation	20.0 years
	Minimum charging state	20 %
Vanadium redox flow	Rated capacity	250 kW
	Nominal voltage's value	700 V
	Nominal capacity's value	2,480 kWh 3,540 Ah
	Cyclic efficiency	70 %
	Peak charging current	290 A
	Peak discharging current	441 A
	Capital cost	\$100,000
	Replacement cost	\$80,000
	Operational-maintenance cost	\$1000/year
	Minimum lifespan of storage system	4.0 years
	Initial Charging state	100 %
	Lifespan of operation	25.0 years
	Minimum charging state	20 %

tariff (\$0.1013 levelized) and operational cost (\$58,830.93) values, thereby, demonstrating its superior economic performance and operating efficiency above the other 3 configuration systems (table 2), respectively.

**APPENDIX**

see Table 5 here.

**REFERENCES**

- [1] G. Liu, B. Zhou, and S. Liao, "Inverting methods for thermal reservoir evaluation of enhanced geothermal system," *Renew. Sustain. Energy Rev.*, vol. 82, pp. 471–476, Feb. 2018, doi: 10.1016/j.rser.2017.09.065.
- [2] V. Khare, S. Nema, and P. Baredar, "Solar-wind hybrid renewable energy system: A review," *Renew. Sustain. Energy Rev.*, vol. 58, pp. 23–33, May 2016, doi: 10.1016/j.rser.2015.12.223.
- [3] R. N. S. R. Mukhtaruddin, H. A. Rahman, M. Y. Hassan, and J. J. Jamian, "Optimal hybrid renewable energy design in autonomous system using iterative-Pareto-fuzzy technique," *Int. J. Electr. Power Energy Syst.*, vol. 64, pp. 242–249, Jan. 2015, doi: 10.1016/j.ijepes.2014.07.030.
- [4] S. Salehin, M. T. Ferdaous, R. M. Chowdhury, S. S. Shithi, M. S. R. B. Rofi, and M. A. Mohammed, "Assessment of renewable energy systems combining techno-economic optimization with energy scenario analysis," *Energy*, vol. 112, pp. 729–741, Oct. 2016, doi: 10.1016/j.energy.2016.06.110.
- [5] M. Mohammadi, R. Ghasempour, F. Razi Astaraei, E. Ahmadi, A. Aligholian, and A. Toopshekan, "Optimal planning of renewable energy resource for a residential house considering economic and reliability criteria," *Int. J. Electr. Power Energy Syst.*, vol. 96, pp. 261–273, Mar. 2018, doi: 10.1016/j.ijepes.2017.10.017.
- [6] Y. He, S. Guo, J. Zhou, F. Wu, J. Huang, and H. Pei, "The quantitative techno-economic comparisons and multi-objective capacity optimization of wind-photovoltaic hybrid power system considering different energy storage technologies," *Energy Convers. Manage.*, vol. 229, Feb. 2021, Art. no. 113779, doi: 10.1016/j.enconman.2020.113779.
- [7] A. Sharma and M. Kolhe, "Techno-economic evaluation of PV based institutional smart micro-grid under energy pricing dynamics," *J. Cleaner Prod.*, vol. 264, Aug. 2020, Art. no. 121486, doi: 10.1016/j.jclepro.2020.121486.
- [8] G. Liu, M. Li, B. Zhou, Y. Chen, and S. Liao, "General indicator for techno-economic assessment of renewable energy resources," *Energy Convers. Manage.*, vol. 156, pp. 416–426, Jan. 2018, doi: 10.1016/j.enconman.2017.11.054.
- [9] R. Hanna, M. Ghonima, J. Kleissl, G. Tynan, and D. G. Victor, "Evaluating business models for microgrids: Interactions of technology and policy," *Energy Policy*, vol. 103, pp. 47–61, Apr. 2017, doi: 10.1016/j.enpol.2017.01.010.
- [10] G. Liu, M. G. Rasul, M. T. O. Amanullah, and M. M. K. Khan, "Techno-economic simulation and optimization of residential grid-connected PV system for the Queensland climate," *Renew. Energy*, vol. 45, pp. 146–155, Sep. 2012, doi: 10.1016/j.renene.2012.02.029.
- [11] M. Elkazaz, M. Sumner, and D. Thomas, "Energy management system for hybrid PV-wind-battery microgrid using convex programming, model predictive and rolling horizon predictive control with experimental validation," *Int. J. Electr. Power Energy Syst.*, vol. 115, Feb. 2020, Art. no. 105483, doi: 10.1016/j.ijepes.2019.105483.
- [12] A. Razmjoo, L. G. Kaigutha, M. A. V. Rad, M. Marzband, A. Davarpanah, and M. Denai, "A technical analysis investigating energy sustainability utilizing reliable renewable energy sources to reduce CO<sub>2</sub> emissions in a high potential area," *Renew. Energy*, vol. 164, pp. 46–57, Feb. 2021, doi: 10.1016/j.renene.2020.09.042.
- [13] A. A. Razmjoo, A. Davarpanah, and A. Zargarian, "The role of renewable energy to achieve energy sustainability in Iran. An economic and technical analysis of the hybrid power system," *Technol. Econ. Smart Grids Sustain. Energy*, vol. 4, no. 1, Apr. 2019, doi: 10.1007/s40866-019-0063-3.
- [14] M. A. Cuesta, T. Castillo-Calzadilla, and C. E. Borges, "A critical analysis on hybrid renewable energy modeling tools: An emerging opportunity to include social indicators to optimise systems in small communities," *Renew. Sustain. Energy Rev.*, vol. 122, Apr. 2020, Art. no. 109691, doi: 10.1016/j.rser.2019.109691.

- [15] F. Fodhil, A. Hamidat, and O. Nadjemi, "Potential, optimization and sensitivity analysis of photovoltaic-diesel-battery hybrid energy system for rural electrification in Algeria," *Energy*, vol. 169, pp. 613–624, Feb. 2019, doi: [10.1016/j.energy.2018.12.049](https://doi.org/10.1016/j.energy.2018.12.049).
- [16] N. Ghorbani, A. Kasaeian, A. Toopshekan, L. Bahrami, and A. Maghami, "Optimizing a hybrid wind-PV-battery system using GA-PSO and MOPSO for reducing cost and increasing reliability," *Energy*, vol. 154, pp. 581–591, Jul. 2018, doi: [10.1016/j.energy.2017.12.057](https://doi.org/10.1016/j.energy.2017.12.057).
- [17] A. M. Eltamaly, M. A. Mohamed, M. S. Al-Saud, and A. I. Alolah, "Load management as a smart grid concept for sizing and designing of hybrid renewable energy systems," *Eng. Optim.*, vol. 49, no. 10, pp. 1813–1828, Dec. 2016, doi: [10.1080/0305215x.2016.1261246](https://doi.org/10.1080/0305215x.2016.1261246).
- [18] M. S. Javed, A. Song, and T. Ma, "Techno-economic assessment of a stand-alone hybrid solar-wind-battery system for a remote island using genetic algorithm," *Energy*, vol. 176, pp. 704–717, Jun. 2019, doi: [10.1016/j.energy.2019.03.131](https://doi.org/10.1016/j.energy.2019.03.131).
- [19] M. Jamshidi and A. Askarzadeh, "Techno-economic analysis and size optimization of an off-grid hybrid photovoltaic, fuel cell and diesel generator system," *Sustain. Cities Soc.*, vol. 44, pp. 310–320, Jan. 2019, doi: [10.1016/j.scs.2018.10.021](https://doi.org/10.1016/j.scs.2018.10.021).
- [20] M. A. M. Ramli, H. R. E. H. Boucekara, and A. S. Alghamdi, "Optimal sizing of PV/wind/diesel hybrid microgrid system using multi-objective self-adaptive differential evolution algorithm," *Renew. Energy*, vol. 121, pp. 400–411, Jun. 2018, doi: [10.1016/j.renene.2018.01.058](https://doi.org/10.1016/j.renene.2018.01.058).
- [21] J. Li, P. Liu, and Z. Li, "Optimal design and techno-economic analysis of a solar-wind-biomass off-grid hybrid power system for remote rural electrification: A case study of West China," *Energy*, vol. 208, Oct. 2020, Art. no. 118387, doi: [10.1016/j.energy.2020.118387](https://doi.org/10.1016/j.energy.2020.118387).
- [22] P. Arévalo, D. Benavides, J. Lata-García, and F. Jurado, "Energy control and size optimization of a hybrid system (photovoltaic-hydrokinetic) using various storage technologies," *Sustain. Cities Soc.*, vol. 52, Jan. 2020, Art. no. 101773, doi: [10.1016/j.scs.2019.101773](https://doi.org/10.1016/j.scs.2019.101773).
- [23] M. C. Argyrou, P. Christodoulides, and S. A. Kalogirou, "Energy storage for electricity generation and related processes: Technologies appraisal and grid scale applications," *Renew. Sustain. Energy Rev.*, vol. 94, pp. 804–821, Oct. 2018, doi: [10.1016/j.rser.2018.06.044](https://doi.org/10.1016/j.rser.2018.06.044).
- [24] M. Aneke and M. Wang, "Energy storage technologies and real life applications—A state of the art review," *Appl. Energy*, vol. 179, pp. 350–377, Oct. 2016, doi: [10.1016/j.apenergy.2016.06.097](https://doi.org/10.1016/j.apenergy.2016.06.097).
- [25] T. Nguyen and R. F. Savinell, "Flow batteries," *Electrochem. Soc. Interface*, vol. 19, no. 3, pp. 54–56, 2010, doi: [10.1149/2.f06103if](https://doi.org/10.1149/2.f06103if).
- [26] Z. Huang, Z. Xie, C. Zhang, S. H. Chan, J. Milewski, Y. Xie, Y. Yang, and X. Hu, "Modeling and multi-objective optimization of a stand-alone PV-hydrogen-retired EV battery hybrid energy system," *Energy Convers. Manage.*, vol. 181, pp. 80–92, Feb. 2019, doi: [10.1016/j.enconman.2018.11.079](https://doi.org/10.1016/j.enconman.2018.11.079).
- [27] W. Liu, F. Zhu, J. Chen, H. Wang, B. Xu, P. Song, P.-A. Zhong, X. Lei, C. Wang, M. Yan, J. Li, and M. Yang, "Multi-objective optimization scheduling of wind-photovoltaic-hydropower systems considering riverine ecosystem," *Energy Convers. Manage.*, vol. 196, pp. 32–43, Sep. 2019, doi: [10.1016/j.enconman.2019.05.104](https://doi.org/10.1016/j.enconman.2019.05.104).
- [28] R. Wang, J. Xiong, M.-F. He, L. Gao, and L. Wang, "Multi-objective optimal design of hybrid renewable energy system under multiple scenarios," *Renew. Energy*, vol. 151, pp. 226–237, May 2020, doi: [10.1016/j.renene.2019.11.015](https://doi.org/10.1016/j.renene.2019.11.015).
- [29] A. Brka, Y. M. Al-Abdeli, and G. Kothapalli, "The interplay between renewables penetration, costing and emissions in the sizing of stand-alone hydrogen systems," *Int. J. Hydrogen Energy*, vol. 40, no. 1, pp. 125–135, Jan. 2015, doi: [10.1016/j.ijhydene.2014.10.132](https://doi.org/10.1016/j.ijhydene.2014.10.132).
- [30] M. J. Mayer, A. Szilágyi, and G. Gróf, "Environmental and economic multi-objective optimization of a household level hybrid renewable energy system by genetic algorithm," *Appl. Energy*, vol. 269, Jul. 2020, Art. no. 115058, doi: [10.1016/j.apenergy.2020.115058](https://doi.org/10.1016/j.apenergy.2020.115058).
- [31] S. Barakat, H. Ibrahim, and A. A. Elbaset, "Multi-objective optimization of grid-connected PV-wind hybrid system considering reliability, cost, and environmental aspects," *Sustain. Cities Soc.*, vol. 60, Sep. 2020, Art. no. 102178, doi: [10.1016/j.scs.2020.102178](https://doi.org/10.1016/j.scs.2020.102178).
- [32] T. Sarkar, A. Bhattacharjee, H. Samanta, K. Bhattacharya, and H. Saha, "Optimal design and implementation of solar PV-wind-biogas-VRFB storage integrated smart hybrid microgrid for ensuring zero loss of power supply probability," *Energy Convers. Manage.*, vol. 191, pp. 102–118, Jul. 2019, doi: [10.1016/j.enconman.2019.04.025](https://doi.org/10.1016/j.enconman.2019.04.025).
- [33] B. K. Das, R. Hassan, M. S. H. K. Tushar, F. Zaman, M. Hasan, and P. Das, "Techno-economic and environmental assessment of a hybrid renewable energy system using multi-objective genetic algorithm: A case study for remote island in Bangladesh," *Energy Convers. Manage.*, vol. 230, Feb. 2021, Art. no. 113823, doi: [10.1016/j.enconman.2020.113823](https://doi.org/10.1016/j.enconman.2020.113823).
- [34] N. M. Kumar, S. S. Chopra, A. A. Chand, R. M. Elavarasan, and G. M. Shafiullah, "Hybrid renewable energy microgrid for a residential community: A techno-economic and environmental perspective in the context of the SDG7," *Sustainability*, vol. 12, no. 10, p. 3944, May 2020, doi: [10.3390/su12103944](https://doi.org/10.3390/su12103944).
- [35] N. Sifakis, S. Konidakis, and T. Tsoutsos, "Hybrid renewable energy system optimum design and smart dispatch for nearly zero energy ports," *J. Cleaner Prod.*, vol. 310, Aug. 2021, Art. no. 127397, doi: [10.1016/j.jclepro.2021.127397](https://doi.org/10.1016/j.jclepro.2021.127397).
- [36] F. Wang, J. Xu, L. Liu, G. Yin, J. Wang, and J. Yan, "Optimal design and operation of hybrid renewable energy system for drinking water treatment," *Energy*, vol. 219, Mar. 2021, Art. no. 119673, doi: [10.1016/j.energy.2020.119673](https://doi.org/10.1016/j.energy.2020.119673).
- [37] M. M. Samy, H. I. Elkhouly, and S. Barakat, "Multi-objective optimization of hybrid renewable energy system based on biomass and fuel cells," *Int. J. Energy Res.*, vol. 45, no. 6, pp. 8214–8230, Sep. 2020, doi: [10.1002/er.5815](https://doi.org/10.1002/er.5815).
- [38] A. H. Eisapour, K. Jafarpur, and E. Farjah, "Feasibility study of a smart hybrid renewable energy system to supply the electricity and heat demand of Eram Campus, Shiraz University; simulation, optimization, and sensitivity analysis," *Energy Convers. Manage.*, vol. 248, Nov. 2021, Art. no. 114779, doi: [10.1016/j.enconman.2021.114779](https://doi.org/10.1016/j.enconman.2021.114779).
- [39] M. Kaur, S. Dhundhara, Y. P. Verma, and S. Chauhan, "Techno-economic analysis of photovoltaic-biomass-based microgrid system for reliable rural electrification," *Int. Trans. Electr. Energy Syst.*, vol. 30, no. 5, Feb. 2020, doi: [10.1002/2050-7038.12347](https://doi.org/10.1002/2050-7038.12347).
- [40] K. Gebrehiwot, M. A. H. Mondal, C. Ringler, and A. G. Gebremeskel, "Optimization and cost-benefit assessment of hybrid power systems for off-grid rural electrification in Ethiopia," *Energy*, vol. 177, pp. 234–246, Jun. 2019, doi: [10.1016/j.energy.2019.04.095](https://doi.org/10.1016/j.energy.2019.04.095).
- [41] P. Malik, M. Awasthi, and S. Sinha, "Study on an existing PV/wind hybrid system using biomass gasifier for energy generation," *Pollution*, vol. 6, no. 2, pp. 325–336, Apr. 2020, doi: [10.22059/poll.2020.293034.719](https://doi.org/10.22059/poll.2020.293034.719).
- [42] J. Tariq, "Energy management using storage to facilitate high shares of variable renewable energy," *Int. J. Sustain. Energy Planning Manag.*, vol. 25, pp. 61–76, Jan. 2020, doi: [10.5278/ijsepm.3453](https://doi.org/10.5278/ijsepm.3453).
- [43] C. P. Nazir, "Solar energy for traction of high speed rail transportation: A techno-economic analysis," *Civil Eng. J.*, vol. 5, no. 7, pp. 1566–1576, Jul. 2019, doi: [10.28991/cej-2019-03091353](https://doi.org/10.28991/cej-2019-03091353).
- [44] A. K. S. Parihar, V. Sethi, and R. Banerjee, "Sizing of biomass based distributed hybrid power generation systems in India," *Renew. Energy*, vol. 134, pp. 1400–1422, Apr. 2019, doi: [10.1016/j.renene.2018.09.002](https://doi.org/10.1016/j.renene.2018.09.002).
- [45] A. S. Aziz, M. F. N. Tajuddin, M. R. Adzman, A. Azmi, and M. A. M. Ramli, "Optimization and sensitivity analysis of standalone hybrid energy systems for rural electrification: A case study of Iraq," *Renew. Energy*, vol. 138, pp. 775–792, Aug. 2019, doi: [10.1016/j.renene.2019.02.004](https://doi.org/10.1016/j.renene.2019.02.004).
- [46] A. Baruah, M. Basu, and D. Amuley, "Modeling of an autonomous hybrid renewable energy system for electrification of a township: A case study for Sikkim, India," *Renew. Sustain. Energy Rev.*, vol. 135, Jan. 2021, Art. no. 110158, doi: [10.1016/j.rser.2020.110158](https://doi.org/10.1016/j.rser.2020.110158).
- [47] S. Sinha and S. S. Chandel, "Analysis of fixed tilt and sun tracking photovoltaic-micro wind based hybrid power systems," *Energy Convers. Manage.*, vol. 115, pp. 265–275, May 2016, doi: [10.1016/j.enconman.2016.02.056](https://doi.org/10.1016/j.enconman.2016.02.056).
- [48] S. Sinha and S. S. Chandel, "Improving the reliability of photovoltaic-based hybrid power system with battery storage in low wind locations," *Sustain. Energy Technol. Assessments*, vol. 19, pp. 146–159, Feb. 2017, doi: [10.1016/j.seta.2017.01.008](https://doi.org/10.1016/j.seta.2017.01.008).
- [49] P. Malik, M. Awasthi, and S. Sinha, "Biomass-based gaseous fuel for hybrid renewable energy systems: An overview and future research opportunities," *Int. J. Energy Res.*, vol. 45, no. 3, pp. 3464–3494, Oct. 2020, doi: [10.1002/er.6061](https://doi.org/10.1002/er.6061).
- [50] A. A. K. Arani, G. B. Gharehpetian, and M. Abedi, "Review on energy storage systems control methods in microgrids," *Int. J. Electr. Power Energy Syst.*, vol. 107, pp. 745–757, May 2019, doi: [10.1016/j.ijepes.2018.12.040](https://doi.org/10.1016/j.ijepes.2018.12.040).



- [51] S. Sinha and S. S. Chandel, "Review of software tools for hybrid renewable energy systems," *Renew. Sustain. Energy Rev.*, vol. 32, pp. 192–205, Apr. 2014, doi: [10.1016/j.rser.2014.01.035](https://doi.org/10.1016/j.rser.2014.01.035).
- [52] C.-T. Tsai, T. M. Beza, E. M. Molla, and C.-C. Kuo, "Analysis and sizing of mini-grid hybrid renewable energy system for islands," *IEEE Access*, vol. 8, pp. 70013–70029, 2020, doi: [10.1109/ACCESS.2020.2983172](https://doi.org/10.1109/ACCESS.2020.2983172).
- [53] O. Ayan and B. E. Turkey, "Techno-economic comparative analysis of grid-connected and islanded hybrid renewable energy systems in 7 climate Regions, Turkey," *IEEE Access*, vol. 11, pp. 48797–48825, 2023, doi: [10.1109/ACCESS.2023.3276776](https://doi.org/10.1109/ACCESS.2023.3276776).
- [54] A. F. Güven, N. Yörükeren, E. Tag-Eldin, and M. M. Samy, "Multi-objective optimization of an islanded green energy system utilizing sophisticated hybrid metaheuristic approach," *IEEE Access*, vol. 11, pp. 103044–103068, 2023, doi: [10.1109/ACCESS.2023.3296589](https://doi.org/10.1109/ACCESS.2023.3296589).
- [55] G. Shafiullah, T. Masola, R. Samu, R. M. Elavarasan, S. Begum, U. Subramaniam, M. F. Romlie, M. Chowdhury, and M. T. Arif, "Prospects of hybrid renewable energy-based power system: A case study, post analysis of chipendeke micro-hydro, Zimbabwe," *IEEE Access*, vol. 9, pp. 73433–73452, 2021, doi: [10.1109/ACCESS.2021.3078713](https://doi.org/10.1109/ACCESS.2021.3078713).
- [56] S. Iqbal, M. U. Jan, Anis-Ur-Rehman, A. U. Rehman, A. Shafiq, H. U. Rehman, and M. Aurangzeb, "Feasibility study and deployment of solar photovoltaic system to enhance energy economics of King Abdullah Campus, University of Azad Jammu and Kashmir Muzaffarabad, AJK Pakistan," *IEEE Access*, vol. 10, pp. 5440–5455, 2022, doi: [10.1109/ACCESS.2022.3140723](https://doi.org/10.1109/ACCESS.2022.3140723).
- [57] H. U. R. Habib, A. Waqar, A. K. Junejo, M. F. Elmorshedy, S. Wang, M. S. Büker, K. T. Akindeji, J. Kang, and Y.-S. Kim, "Optimal planning and EMS design of PV based standalone rural microgrids," *IEEE Access*, vol. 9, pp. 32908–32930, 2021, doi: [10.1109/ACCESS.2021.3060031](https://doi.org/10.1109/ACCESS.2021.3060031).
- [58] V. Vichit-Vadakan. (Jan. 17, 2018). *Koh Chang to Koh Kood: Island-Hopping Around Eastern Thailand*. Guardian. [Online]. Available: <https://www.theguardian.com/travel/2018/jan/17/koh-chang-koh-kood-island-hopping-thailand-quiet-beaches>
- [59] Global Solar Atlas. (2022). *Global Solar Atlas 2.0, a Free, Web-Based Application is Developed and Operated by the Company Solargis SRO on Behalf of the World Bank Group, Utilizing Solargis Data, With Funding Provided by the Energy Sector Management Assistance Program (ESMAP)*. Accessed: Nov. 10, 2023. [Online]. Available: <https://globalsolaratlas.info/>
- [60] B. N. Alhasnawi, B. H. Jasim, A. M. Jasim, V. Bureš, A. N. Alhasnawi, R. Z. Homod, M. R. M. Alsemawai, R. Abbassi, and B. E. Sedhom, "A multi-objective improved cockroach swarm algorithm approach for apartment energy management systems," *Information*, vol. 14, no. 10, p. 521, Sep. 2023, doi: [10.3390/info14100521](https://doi.org/10.3390/info14100521).
- [61] Earth System Science Data. (Sep. 27, 2023). *Prediction Of Worldwide Energy Resources (POWER)*[*Earthdata*]. Accessed: Jan. 18, 2024. [Online]. Available: <https://www.earthdata.nasa.gov/technology/prediction-worldwide-energy-resources-power>
- [62] *HOMER Energy Support Center*. Accessed: Jan. 18, 2024. [Online]. Available: <https://usersupport.homerenergy.com/s/article/wind-power-output-in-homer>
- [63] M. M. Rahman, E. Gemechu, A. O. Oni, and A. Kumar, "The development of a techno-economic model for the assessment of the cost of flywheel energy storage systems for utility-scale stationary applications," *Sustain. Energy Technol. Assessments*, vol. 47, Oct. 2021, Art. no. 101382, doi: [10.1016/j.seta.2021.101382](https://doi.org/10.1016/j.seta.2021.101382).
- [64] *Biomass Database Potential in Thailand*[*Department of Alternative Energy Development and Efficiency*]. Accessed: Jan. 18, 2024. [Online]. Available: <http://weben.dede.go.th/webmax/content/biomass-database-potential-thailand>
- [65] P. Malik, M. Awasthi, and S. Sinha, "A techno-economic investigation of grid integrated hybrid renewable energy systems," *Sustain. Energy Technol. Assessments*, vol. 51, Jun. 2022, Art. no. 101976, doi: [10.1016/j.seta.2022.101976](https://doi.org/10.1016/j.seta.2022.101976).
- [66] G. Mathesh and R. Saravanakumar, "A novel intelligent controller-based power management system with instantaneous reference current in hybrid energy-fed electric vehicle," *IEEE Access*, vol. 11, pp. 137849–137865, 2023, doi: [10.1109/ACCESS.2023.3339249](https://doi.org/10.1109/ACCESS.2023.3339249).



**OLUWASEUN OLANREWAJU AKINTE** received the Bachelor of Science degree in electrical and electronic engineering from Olabisi Onabanjo University, Ago-Iwoye, Nigeria, in 2010, and the Master of Science degree in electrical and electronic engineering from Coventry University, U.K., in 2016. He is currently pursuing the Ph.D. degree in energy and materials engineering with the Rajamangala University of Technology Thanyaburi, Thailand. His research interests include power system technology, hybrid storage systems, hybrid renewable energy sources, and smart grid networks.



**BOONYANG PLANGKLANG** received the B.Eng. degree in electrical engineering from the Rajamangala University of Technology Thanyaburi (RMUTT), Thailand, in 1996, the Diploma degree in instrumentation from Northern Alberta Institute of Technology (NAIT), Edmonton, Alberta, Canada, in 1997, the Master of Science degree in electronics system and engineering management from the Division Soest, University of Paderborn, Germany, with the cooperation of Bolton Institute of Higher Education, U.K., from DAAD Scholarship, in 2001, and the Dr.-Ing. degree in electrical engineering from the University of Kassel, Germany, in 2005. He is currently an Associate Professor with the Department of Electrical Engineering, RMUTT.

...